ESCOLA SUPERIOR DE TECNOLOGIA DA SAÚDE DE LISBOA
INSTITUTO POLITÉCNICO DE LISBOA

INSTITUTO POLITÉCNICO DE LISBOA

ESCOLA SUPERIOR DE TECNOLOGIA DA SAÚDE DE LISBOA

VARIAÇÃO DA INTENSIDADE DE SINAL EM SEQUÊNCIAS DE RESSONÂNCIA MAGNÉTICA CARDÍACA, NO CONTEXTO DE MIOCARDIOPATIA HIPERTRÓFICA E MIOCARDITE

SIGNAL INTENSITY VARIATION IN CARDIAC MAGNETIC RESONANCE SEQUENCES IN THE CONTEXT OF HYPERTROPHIC CARDIOMYOPATHY AND MYOCARDITIS

PATRÍCIA ANDREIA BRANDÃO BECO

ADVISORS:

MARIA JOÃO FURTADO RAMINHAS CARAPINHA, PhD – ESTeSL- Escola Superior de Tecnologia da Saúde de Lisboa, Instituto Politécnico de Lisboa

SANDRA TECELÃO, PhD - Akershus University Hospital

HUGO MARQUES, PhD - Hospital da Luz, Faculdade de Medicina da Universidade Católica

Master's Degree in Radiation Applied to Health Technologies

Lisbon, 2024

INSTITUTO POLITÉCNICO DE LISBOA

ESCOLA SUPERIOR DE TECNOLOGIA DA SAÚDE DE LISBOA

VARIAÇÃO DA INTENSIDADE DE SINAL EM SEQUÊNCIAS DE RESSONÂNCIA MAGNÉTICA CARDÍACA, NO CONTEXTO DE MIOCARDIOPATIA HIPERTRÓFICA E MIOCARDITE

SIGNAL INTENSITY VARIATION IN CARDIAC MAGNETIC RESONANCE SEQUENCES IN THE CONTEXT OF HYPERTROPHIC CARDIOMYOPATHY AND MYOCARDITIS

PATRÍCIA ANDREIA BRANDÃO BECO

ADVISORS:

MARIA JOÃO FURTADO RAMINHAS CARAPINHA, PhD – ESTeSL- Escola Superior de Tecnologia da Saúde de Lisboa, Instituto Politécnico de Lisboa

SANDRA TECELÃO, PhD - Akershus University Hospital

HUGO MARQUES, PhD - Hospital da Luz, Faculdade de Medicina da Universidade Católica

JURY:

PRESIDENT – MARIA MARGARIDA RIBEIRO, PhD - ESTeSL- Escola Superior de Tecnologia da Saúde de Lisboa, Instituto Politécnico de Lisboa

ARGUENT - RITA GOUVEIA NUNES, **PhD** – LaSEEB - Evolutionary Systems and Biomedical Engineering Lab, Instituto Superior Técnico, Universidade de Lisboa

ADVISOR - **SANDRA TECELÃO, PhD -** Akershus University Hospital

Master's Degree in Radiation Applied to Health Technologies

(this version includes the critiques and suggestions made by the jury)

Lisbon, 2024

Document written in English

ACKNOWLEDGMENTS

I would like to express my gratitude towards my advisor Doctor Professor Maria João Carapinha, for the availability and clearing of doubts.

To my advisor Doctor Professor Sandra Tecelão for all the guidance, essential exchange of ideas, and for finding the time to help even when that was almost impossible.

I would also want to express my sincere appreciation to Doctor Professor Hugo Marques, also my advisor and Radiologist from Hospital da Luz, for the clinical insights and feedback, and extend my heartfelt thanks to another Doctor, António Ferreira, for all the initial support and help to find the data available.

A big thanks to my work colleagues who have always motivated and supported me during the development of the dissertation.

To my parents and brother, a heartfelt thanks, for being my safe place every day and never letting me quit, always motivating me to be more and better. Thank you for educating me and encouraging me to continue my studies. I also thank my cousin Bruno, who helped me with his experience on this matter and with the pressure I felt in the end.

Finally, I would like to acknowledge with deep gratitude the support of all my friends, my longtime friends, and the ones I had the pleasure to live this experience with. This two-year journey was beautiful, and I am grateful for it.

ABSTRACT

Cardiovascular diseases are a leading cause of morbidity and mortality globally. Cardiac magnetic resonance is a non-invasive, ionizing radiation-free imaging method essential for the diagnosis and monitoring of cardiovascular diseases. Techniques like Late Gadolinium Enhancement, T1 Mapping, and CINE imaging are valuable for evaluating heart structure, function, and pathology. Late Gadolinium Enhancement, while effective, requires contrast agents, which may accumulate in the body and cause complications in patients with chronic kidney disease. This study investigates the possibility of using T1 Mapping and/or CINE images as the first triage to detect possible candidates for Late Gadolinium Enhancement images.

METHODS: A total of 36 individuals (18 LGE+ and 18 LGE-) undergoing CMR for myocarditis or Hypertrophic Cardiomyopathy were analyzed. Demographic data were collected, and mean values were recorded. Qualitative and quantitative analyses were performed on T1 Mapping and CINE images to assess their sensitivity, specificity, accuracy, and precision in detecting myocardial enhancement.

RESULTS: T1 Mapping has shown potential in identifying changes in the myocardium, but with variations in sensitivity and less consistency in detecting pathological patterns when compared to CINE Imaging, which has shown greater consistency, with 72% sensitivity in detecting affected areas. Blind test analysis showed that 73% of patients had no lesions identified and were negative, avoiding the use of contrast. The physician was correct in 87.5% of positive cases, identifying at least one positive image modality of hypersignal, ensuring that these patients received contrast correctly and only 12.5% would not need it.

DISCUSSION/CONCLUSIONS: The results show that T1 mapping and CINE images are promising as initial triage tools for detecting Myocarditis and HCM. This would exclude many healthy patients from contrast-enhanced examinations, reducing risks and costs. This would increase efficiency, allowing for more scans in less time, crucial during gadolinium shortages. The analysis also highlights the importance of machine learning (ML) software to better detect the signal intensity variations.

KEYWORDS: T1 mapping; Late Gadolinium Enhancement; CINE imaging; Cardiac MRI, Hypertrophic Cardiomyopathy, Myocarditis.

RESUMO

As doenças cardiovasculares são uma das principais causas de morbilidade e mortalidade a nível mundial. A ressonância magnética cardíaca é um método de imagiologia não invasivo, isento de radiação ionizante, essencial para o diagnóstico e monitorização de doenças cardiovasculares. Técnicas como o realce tardio com gadolínio, o mapeamento T1 e a imagiologia CINE são valiosas para avaliar a estrutura, a função e a patologia do coração. O realce tardio com gadolínio, embora eficaz, requer agentes de contraste, que se podem acumular no organismo e causar complicações em doentes com doença renal crónica. Este estudo investiga a possibilidade de utilizar o mapeamento T1 e/ou imagens CINE como primeira triagem para detetar possíveis candidatos a imagens de realce tardio com gadolínio.

MÉTODOS: Foram analisados 36 indivíduos (18 com LGE+ e 18 com LGE-) submetidos a RMC por miocardite ou CMH. Foram recolhidos dados demográficos e registados os valores médios. Foram realizadas análises qualitativas e quantitativas das imagens de mapeamento T1 e CINE para avaliar a sua sensibilidade, especificidade, acurácia e precisão na deteção do realce miocárdico.

RESULTADOS: O T1 Mapping demonstrou potencial na identificação de alterações no miocárdio, mas com variações de sensibilidade e menor consistência na deteção de padrões patológicos quando comparado com o CINE Imaging, que demonstrou maior consistência, com 72% de sensibilidade na deteção de áreas afetadas. A análise do teste cego mostrou que 73% dos pacientes não tiveram lesões identificadas e foram negativos, evitando o uso de contraste. O médico acertou em 87,5% dos casos positivos, identificando pelo menos uma modalidade de imagem positiva de hipersinal, assegurando que estes doentes recebiam corretamente o contraste e que apenas 12,5% não necessitariam dele.

DISCUSSÃO/CONCLUSÕES: Os resultados mostram que o mapeamento T1 e as imagens CINE são promissores como ferramentas de triagem inicial para a deteção de miocardite e HCM. Isto excluiria muitos doentes saudáveis dos exames com contraste, reduzindo os riscos e os gastos associados. Isto aumentaria a eficiência, permitindo efetuar mais exames em menos tempo, o que é crucial durante a escassez de gadolínio.

A análise também destaca a importância do software de aprendizagem automática (ML) para detetar melhor as variações de intensidade do sinal.

PALAVRAS-CHAVE: Mapeamento T1; realce tardio por gadolínio; imagem CINE; RM cardíaca; Cardiomiopatia Hipertrófica; Miocardite.

TABLE OF CONTENTS

TABLE OF FIGURES

TABLE INDEX

LIST OF ABBREVIATIONS

2D – Bidimensional

3D – Tridimensional

AHA – American Heart Association

AM – Acute myocarditis

BOLD – Blood Oxygen Level Dependent

bSSFP - Balanced Steady-State Free Precession

CM – Cardiomyopathy

CMR – Cardiac Magnetic Resonance

CSF – Cerebrospinal Fluid

DW – Diffusion Weighted

EPI – Echo-planar image

EV – Ejection fraction

FA – Flip Angle

FID – Free Induction Decay

FLASH - Fast Low Angle Shot

FISP – Fast Imaging with Steady-State Precession

FN – False Negative

FP – False Positive

GBCAs – Gadolinium Based Contrast Agents

GRASS – Gradient Recalled Acquisition in Steady State

GRE – Gradient Echo

HCM – Hypertrophic Cardiomyopathy

ICM – Inflammatory Cardiomyopathy

IR – Inversion Recovery

LE – Late Enhancement

LGE – Late gadolinium Enhancement

LGE+ – Positive patient for LE

LGE- – Negative patient for LE

LL – Look-Locker

LV – Left Ventricle

ML – Machine Learning

MI – Myocardial infarction

MOLLI– Modified Look-Locker Inversion

MPC – Myocardium Perfusion Contrast

MRI – Magnetic Resonance Imaging

ms – Milliseconds

PACS – Picture Archiving and Communication System

PS – Pulse Sequences

PSIR – Phase-Sensitive Inversion Recovery

RF – Radiofrequency

ROI – Region of interest

SASHA – Saturation recovery single-shot Acquisition

SCD – Sudden cardiac death

SE – Spin Echo

shMOLLI – Shortened MOLLI

SNR – Signal Noise Rate

SPGR – Spoiled Gradient-Recalled

SSFP – Steady-State Free Precession

SR – Saturation recovery

T – Tesla

T1 – Longitudinal relaxation time

T2 – Transversal relaxation time

TI – Inversion Time

TE – Echo time

TN – True Negative

TNR – True Negative Rate

TP – True Positive

TPR – True Positive Rate

TR – Repetition time

TRUFI – True Fast Imaging with Steady-State Free Precession

TSE – Turbo Spin-Echo

ρH – Proton density

INTRODUCTION

One of the greatest strengths of Cardiovascular Magnetic Resonance (CMR) is its ability to accurately characterize cardiac tissue and detect diseases. In recent years, this characterization has evolved from a purely qualitative approach to a more objective assessment through parametric T1 and T2 mapping. These advanced imaging techniques enable precise measurement of edema, inflammation, scarring, and, most importantly, systemic myocardial changes in the extracellular space - many of which were previously undetectable using conventional Magnetic Resonance Imaging (MRI) or other imaging methods. The rapid adoption of these innovations has significantly enhanced the diagnostic and prognostic capabilities of cardiologists across various cardiovascular conditions. (1) MRI Techniques such as Late Gadolinium Enhancement (LGE), T1 Mapping, and CINE imaging have become essential in cardiovascular studies, offering a comprehensive evaluation of the heart's structure, function, and physiology. Together, these modalities play a critical role in the early detection, characterization, and monitoring of cardiovascular diseases, supporting clinical decision-making and optimizing treatment strategies.

Relevance of the Study

Late Gadolinium Enhancement (LGE) is the gold standard non-invasive imaging technique for assessing myocardial scarring. However, it has notable limitations, including challenges in differentiating scar tissue from healthy myocardium and its reduced sensitivity in detecting diffuse fibrosis. Additionally, the interpretation of gadolinium-enhanced signal intensities is hindered by their arbitrary scale, making longitudinal comparisons difficult. Furthermore, the accuracy of LGE imaging is influenced not only by technical parameters during acquisition but also by the subjectively defined intensity thresholds, which may impact consistency and reproducibility. (1)

T1 Mapping provides critical insights into the composition and viability of cardiac tissue, facilitating the detection and characterization of pathological conditions such as fibrosis, edema, myocardial infarction, inflammation, and cardiac amyloidosis. (2)

CINE imaging plays a pivotal role in the functional assessment of the heart by enabling real-time visualization and analysis of cardiac motion. It provides essential information on contractility, ventricular function, and cardiac anatomy, making it indispensable for the

diagnosis and monitoring of conditions such as heart failure, valvular disease, and structural abnormalities. Clinically, CINE imaging is widely used to assess both morphological and functional cardiac parameters, with a particular focus on detecting ventricular dysfunction and pericardial effusion. (3) Unlike conventional T2-weighted imaging, CINE imaging offers superior robustness and high-fidelity images, benefiting from its intrinsic T2/T1-weighted contrast, which may enhance the detection of active inflammatory processes and myocardial fibrosis. Studies, including that of Collidge et al., suggest that CINE imaging, as a non-contrast-based modality, represents a promising alternative to LGE, particularly in patients with severe renal impairment where gadolinium administration is contraindicated. (4) Despite its advantages, CINE imaging has not yet been fully exploited for tissue characterization, primarily due to its limited interpretability through conventional visual assessment. However, emerging research utilizing texture analysis techniques suggests that CINE imaging may reveal pathological patterns not easily discernible to the human eye. (3)

It is therefore important to deepen the knowledge in this area and, with this study, to really investigate both, visually and quantitatively, the possibility of using the CINE technique and/or T1 Mapping as a viable alternative to replace LGE techniques and to discuss the clinical implications and limitations of applying different imaging techniques in medical practice, considering aspects such as diagnostic accuracy, cost-effectiveness, and availability.

Study Outline

This thesis is organized in 4 chapters. Chapter 1 presents a theoretical background, including a literature review of HCM pathology, Myocarditis, Fundamentals of MRI, and a description of the LGE, T1 mapping and CINE imaging sequences used in this study. Chapter 2 describes the study and its methods. Chapters 3 and 4 present the results and discussion.

OBJECTIVES

The main objective of this study is to compare the MRI techniques: LGE, T1, and CINE Imaging in CMR, in the context of cardiovascular diseases such as myocarditis and HCM, to see if it is possible to use T1 Mapping and/or CINE images as the first triage to detect possible candidates for LGE images.

The most specific objectives are:

1- Qualitative comparative analysis of the LGE, CINE, and T1 images.
2- Quantitative comparative analysis of T1 maps and LGE+ ROIs in patients with disease.
3- Quantitative comparative analysis of T1 maps and LGE images per segment in patients with disease.
4- Quantitative comparative analysis of CINE images and LGE+ ROIs in patients with disease.
5- Quantitative comparative analysis of CINE and LGE images per segment in patients with disease.
6- “Blind” visual analysis for validation of the presented results.

CHAPTER 1 THEORETICAL BACKGROUND

1.1 FUNDAMENTALS OF MAGNETIC RESONANCE IMAGING

Magnetic Resonance Imaging (MRI) is a non-invasive imaging modality widely employed in medical diagnostics to obtain high-resolution anatomical and functional images. The technique is based on the interaction of hydrogen nuclei within biological tissues with a strong external magnetic field and radiofrequency (RF) pulses, allowing for precise tissue characterization. (5)

In more detail, the hydrogen nuclei present in the human body, mainly in adipose tissue and body's water content (6), have a property called "spin", which generates a magnetic field. Under normal conditions, these spins are randomly oriented, resulting in no net magnetization. When a patient is placed inside the MRI scanner, a strong external magnetic field is applied. This field aligns the spins of the hydrogen nuclei in two possible directions: parallel or antiparallel to the field. By applying a radiofrequency (RF) pulse with a specific frequency (Larmor frequency), the hydrogen nuclei absorb energy and change their spin state. This phenomenon is known as resonance. After the RF pulse is switched off, the hydrogen nuclei return to their equilibrium state, releasing the absorbed energy in the form of radio signals. This process is divided into two types: Longitudinal Relaxation (T1): the time required for the spins to realign with the external magnetic field, and Transverse Relaxation (T2): the time needed for the spins to lose phase coherence with each other. (1,7)

The MRI scanner has coils with gradients oriented in the x, y, and z planes, as well as a signal-receiving antenna, which captures the energy emitted by the hydrogen nuclei during relaxation, locates it spatially, and converts it into an image using the Fourier transform. These gradients vary the intensity of the magnetic field along different axes, allowing the exact location of the resonance signals. (7)

1.1.1 WEIGHTED IMAGES: T1 AND T2

One of the greatest advantages of MRI is the ability to generate tissue contrast, which is closely related to the fact that different tissues have different T1 and T2 values.

T1-weighted images are obtained by using short TR and short TE values, optimizing the contrast based on T1 relaxation differences among tissues. Tissues with shorter T1 relaxation times recover longitudinal magnetization more rapidly and appear hyperintense (bright), whereas tissues with longer T1 relaxation times appear hypointense (dark). In T1-weighted images: fat exhibits a high signal intensity due to its short T1 relaxation time; Water-containing structures, such as cerebrospinal fluid (CSF),

appear dark due to their long T1 relaxation times; Muscle and soft tissues typically present with intermediate signal intensity. (1) T1-weighted imaging is beneficial for anatomical assessment, detecting hemorrhages, fat infiltration, and evaluating post-contrast enhancement when gadolinium-based contrast agents (GBCAs) are administered.

T2-weighted images are generated by employing long TR and long TE values, which accentuate differences in T2 relaxation times. Tissues with prolonged T2 relaxation retain transverse magnetization longer and appear hyperintense, whereas tissues with shorter T2 relaxation times decay more rapidly and appear hypointense. In T2-weighted images: water-rich tissues, such as edema, inflammation, or cystic structures, exhibit high signal intensity; fat appears darker compared to T1-weighted imaging due to its shorter T2 relaxation time; muscle and normal soft tissues display intermediate signal intensities. (6,7) T2-weighted imaging is particularly valuable for detecting pathological changes, including fluid accumulation, edema, ischemic injury, and demyelination. It is widely used in neuroimaging, musculoskeletal MRI, and cardiovascular applications to assess myocardial tissue alterations.

Thus, by selectively manipulating TR and TE parameters, radiologists can tailor MRI sequences to optimize tissue contrast for specific diagnostic needs. The combination of T1- and T2-weighted imaging enhances the ability to differentiate normal from pathological tissues, making MRI a powerful modality for comprehensive tissue characterization. (7)

1.1.2 MRI PULSE SEQUENCES

An MRI pulse sequence (PS) is a programmed set of changing magnetic gradients. Each sequence will have several parameters, and multiple sequences group into an MRI protocol. (8)

MRI sequences can be classified using different criteria, primarily based on their underlying pulse mechanisms, such as spin echo (SE) or inversion recovery (IR). However, for individuals without specialized training in radiology, a more intuitive approach to categorizing these sequences is by their image contrast properties (e.g., T1-weighted or T2-weighted) and specific enhancements, such as fat suppression or gadolinium contrast administration. Broadly, MRI sequences can be divided into several main categories, including spin echo (SE), inversion recovery (IR), gradient echo (GRE), diffusion-weighted imaging (DWI), saturation recovery (SR), echo-planar imaging (EPI), and spiral sequences. PS can be broadly grouped as follows: spin echo (SE), inversion

recovery (IR), gradient echo (GRE), diffusion-weighted (DW), saturation recovery (SR), echo-planar pulse (EPI), and spiral pulse sequences. (8) In this study, just the two main groups of PS are specified: SE and GRE sequences. Acquisition can be two-dimensional (2D), with one section acquired at a time, or three-dimensional (3D), with a volume of data acquired in a single acquisition. (9)

SE pulse sequences are one of the first MRI pulse sequences developed and still widely used. The timing of the pulse sequence can be adjusted to obtain T1-weighted, proton density, and T2-weighted images. Double echo and multi-echo sequences can simultaneously obtain proton density and T2-weighted images. The two variables of interest in spin-echo sequences are repetition time (TR) and echo time (TE). All spin-echo sequences include a 90-degree selective pulse followed by one or more 180-degree refocusing pulses.

The intensity of the MRI signal produced using a SE sequence is proportional to the proton density (ρH), TR, T1, TE, and T2. (8)

GRE pulse sequences are an alternative technique to SE sequences differing from it in two principal points: utilization of gradient fields to generate transverse magnetization and flip angles of less than 90°. Gradients will be used to return this in-phase movement (called positive gradients or rewind) or remove the in-phase movement of the spins (negative gradient or spoilers). (10) Compared to the SE sequences, the GRE is more versatile. The fundamental sequence can be modified by incorporating dephasing or rephasing gradient pulses at the end of the cycle. Additionally, beyond the standard parameters of repetition time (TR) and echo time (TE), another crucial factor influencing image contrast is the flip angle (FA), which determines the degree of spin rotation induced by the radiofrequency pulse. (8)

The FA is usually at or close to 90 degrees for a SE sequence but is less on this sequence, commonly varying over a range of 10 to 80 degrees (usually denoted by α). For the basic GRE sequence FLASH, the larger flip angles give more T1 weighting to the image, and the smaller flip angles give more T2, or actually T2* weighting, to the images. (8)

The GRE is generated by the frequency-encode gradient, except that it is used twice in succession, and opposite directions: it is used in reverse at first to enforce transverse dephasing of spinning protons, and then right after, it is used as a readout gradient (like

in SE MRI) to re-align the dephased protons and hence acquire signal (8), this process is called gradient echo.

Due to the use of a low flip angle (FA), a portion of the longitudinal magnetization is preserved, unlike the 90° pulse in spin echo (SE) sequences, which completely nullifies longitudinal magnetization. Consequently, the recovery time for longitudinal magnetization between successive pulses is significantly reduced, enabling faster image acquisition in gradient echo (GRE) sequences. Another key characteristic of GRE imaging is that signal dephasing occurs primarily due to T2* decay, which happens more rapidly than the T2 decay observed in SE sequences. This results in shorter echo times (TE) but also increases sensitivity to magnetic field inhomogeneities, leading to greater susceptibility artifacts, especially in areas affected by blood degradation products or metallic implants. (8)

Different GRE techniques produce varying tissue contrast characteristics. Sequences like GRASS (Gradient Recalled Acquisition in Steady State) and FISP (Fast Imaging with Steady-State Precession) exhibit more complex contrast behavior compared to FLASH (Fast Low Angle Shot). While FLASH and SPGR (Spoiled Gradient-Recalled) are preferred when acquisition time is less constrained, GRASS and FISP offer a higher signal-to-noise ratio (SNR) at shorter repetition times (TR), making them particularly useful in breath-hold imaging protocols. (8) TRUFI (True Fast Imaging with Steady-State Free Precession) is another GRE-based sequence that enhances the visibility of blood vessels and fluid-filled structures due to its unique contrast properties. (11)

In GRE sequences, spins are refocused by altering their phase rather than applying a 180° refocusing pulse, as seen in SE sequences. This gradient-based refocusing process is much faster, contributing to the efficiency of GRE imaging. However, one notable drawback of GRE sequences is their susceptibility to static magnetic field inhomogeneities, which can lead to pronounced magnetic susceptibility artifacts, making them more sensitive to distortions than SE sequences. (8)

1.2 CARDIAC MAGNETIC RESONANCE

Cardiac Magnetic Resonance (CMR) is a non-invasive imaging method, without the use of radiation and with the ability to take slices in multiple planes, with high spatial and temporal resolution, which gives it greater diagnostic capacity. (12) It also can characterize tissue, particularly in assessing perfusion changes and detecting edema and areas of myocardial fibrosis. Thus, CMR has emerged as a new reference test for

diagnosing and assessing cardiac function, with clear advantages in etiological diagnosis. (1,9)

1.2.1 ANATOMY AND PHYSIOLOGY OF THE HEART

The heart is made up of 4 chambers, 2 atria, and 2 ventricles. De-oxygenated blood returns to the right side of the heart via venous circulation, it is pumped into the right ventricle and then to the lungs where carbon dioxide is released, and oxygen is absorbed. The oxygenated blood then travels back to the left side of the heart into the left atrium, then into the left ventricle from where it is pumped into the aorta and arterial circulation (13) (see Figure 1:1).

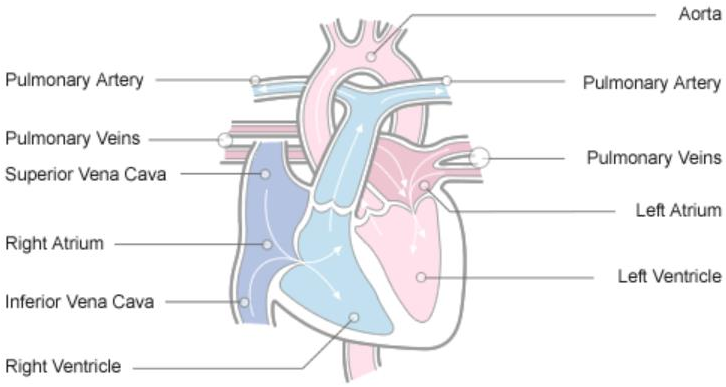

Figure 1:1 - Fontal view representing the passage of blood through the heart (14)

The pressure created in the arteries by the contraction of the left ventricle is the Systolic blood pressure. Once the left ventricle has fully contracted it begins to relax and refill with blood from the left atrium. The pressure in the arteries falls whilst the ventricle refills and this is the Diastolic blood pressure. The atrioventricular septum completely separates the 2 sides of the heart. (13)

The volume of ejected blood, as well as what remains in the chambers after each systole and diastole, are important measurements used in clinical practice as indicators of cardiac function. Thus, one of the measures that Myocardium Perfusion Contrast (MPC) allows us to access is the Ejection Fraction (EV), which corresponds to the percentage of blood that is ejected from the ventricles in each systole. (10)

Therefore, whenever physiological situations require an increase in blood supply to the tissues, the heart must increase its function, with a consequent increase in its own irrigation and oxygen supply. For the heart to respond positively to this demand, changes

in coronary flow are necessary. Pathological changes in the diameter of the coronary arteries can restrict the blood supply to the myocardium (especially in situations of greater cardiac demand), causing myocardial physiology and viability to become compromised.

The myocardium, the muscular layer of the heart, plays a fundamental role in cardiac contraction, enabling the heart to function as an efficient pump. It is primarily composed of cardiomyocytes, specialized muscle cells with unique structural and physiological properties that generate the contractile force necessary to sustain adequate blood circulation and tissue perfusion. The myocardium is extensively supplied by coronary vasculature, supported by cardiac lymphatics, and regulated by autonomic innervation, ensuring optimal function under varying physiological demands. Given its critical role in cardiovascular health, a comprehensive understanding of myocardial anatomy and function is essential for diagnosing and managing a wide range of cardiac conditions. (14)

Three distinct layers comprise the heart walls, from inner to outer: Endocardium, Myocardium, and Epicardium (see Figure 1:2).

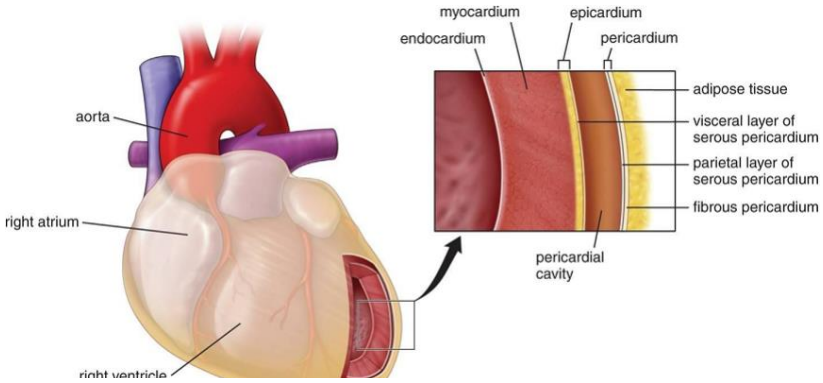

Figure 1:2 - The passage of blood through the heart (15)

The myocardium constitutes the middle and thickest layer of the heart wall, positioned between the endocardium, which lines the inner chambers, and the epicardium, the protective outer layer of the heart. Histologically, it is composed of cardiomyocytes—specialized muscle cells with distinct structural and functional properties that enable contraction. These cells form an interconnected network, allowing the myocardium to function as a syncytium, facilitating rapid and coordinated contractions essential for

effective blood circulation. The myocardium's contractile activity is driven by electrochemical gradients, which generate the force required for each heartbeat. (14)

The myocardial layer is present in all four heart chambers; however, it is significantly thicker in the ventricles compared to the atria. This structural difference reflects the varying levels of contractile force needed, as the ventricles must generate higher pressure to propel blood through the systemic and pulmonary circulations, whereas the atria require less force to transfer blood into the ventricles.

1.2.2 ANATOMICAL PLANES – ORIENTATION OF THE CARDIAC AXIS AND SEGMENTATION OF THE LEFT VENTRICLE

The two main coordinate systems used in CMR include the body planes and the cardiac planes. The anatomical planes are oriented orthogonally to the long axis of the body and are axial, sagittal, and coronal (Figure 1:3). They are used to obtain the scanning images that provide a qualitative description of cardiac morphology. (15)

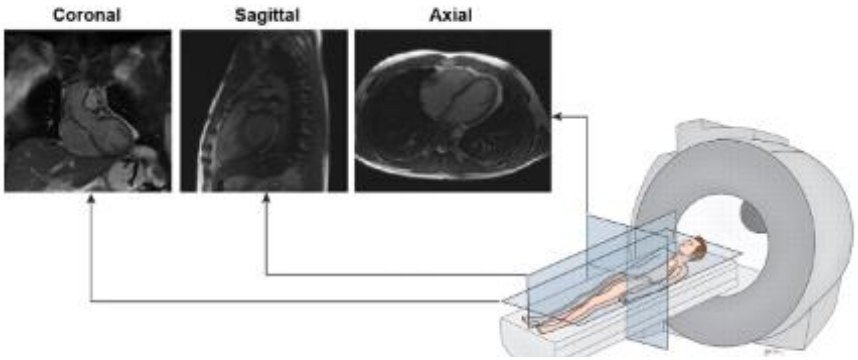

Figure 1:3 - Orientation of major body planes with respect to patient and their corresponding appearance (35)

The standard cardiac planes, illustrated in Figure 1:4, are established using the scout images and include a short axis, horizontal long axis (four-chamber view), and vertical long axis (two-chamber view). These planes are defined along a line extending from the cardiac apex to the center of the mitral valve (long axis of the heart) using the axial plane images of the body.

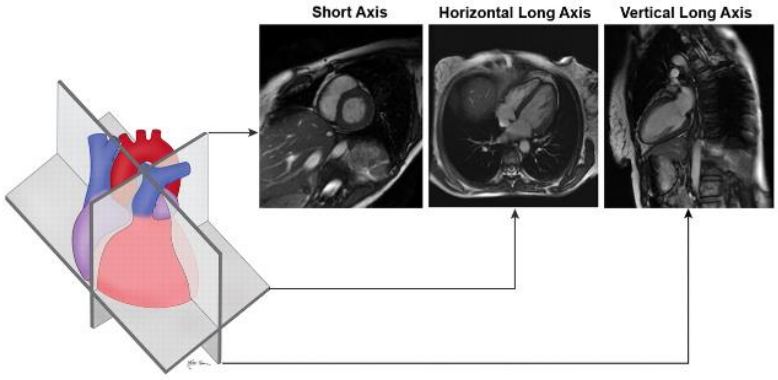

Figure 1:4 - Orientation of major cardiac planes concerning heart and their corresponding appearance (35)

The short-axis plane is obtained perpendicular to the long axis of the heart so that images can be acquired from the base to the apex (16), as it is represented in Figure 1:5.

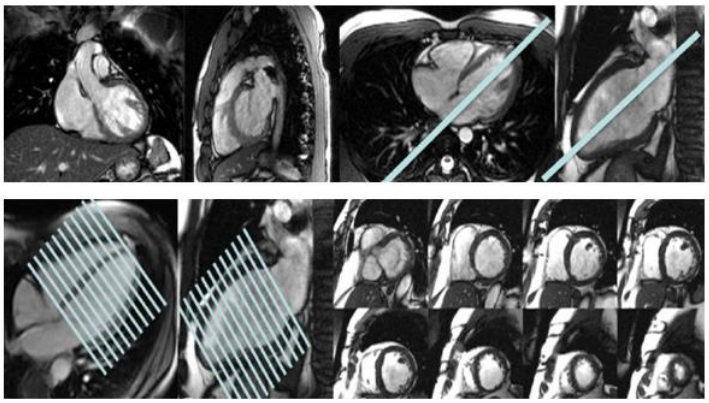

Figure 1:5 – Representation of how to obtain a short-axis cardiac plane.

This makes it possible to assess the myocardium in its basal, medial, and apical portions, the size of the left ventricle, and quantify cardiac function and the contractility of the ventricle. (17)

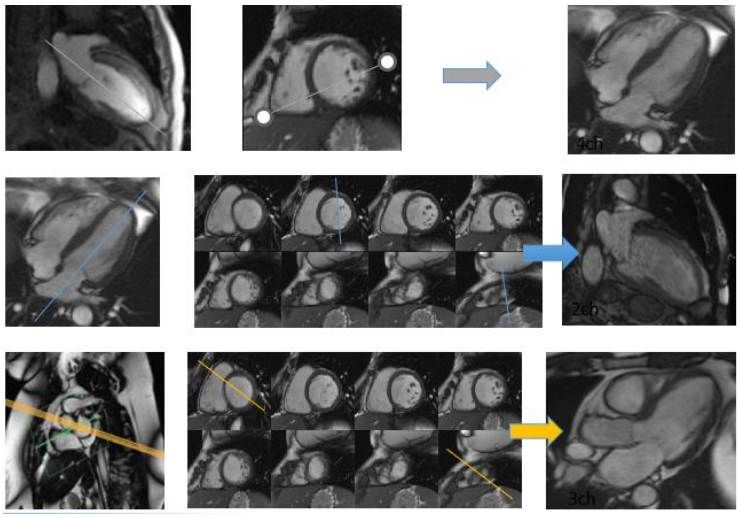

Figure 1:6 – Representation of how to obtain a Vertical and Horizontal long axis cardiac plane.

The horizontal long axis is generated by selecting the horizontal plane that is perpendicular to the short axis. It crosses the four heart chambers, allowing their size and valve position to be assessed. It also allows the mitral and tricuspid valves to be assessed simultaneously, among other anatomical structures. The vertical long axis is defined along the vertical plane orthogonal to the short axis. It is parallel to the sagittal plane oriented along the axis of the heart. It can be acquired in two directions, to analyze the inflow tract of the ventricle or the outflow tract. (16) Both representations are illustrated in Figure 1:6.

For a better understanding of the images analyzed in this study, a normal CMR anatomy of the heart in a short-axis view is illustrated in Figure 1:7.

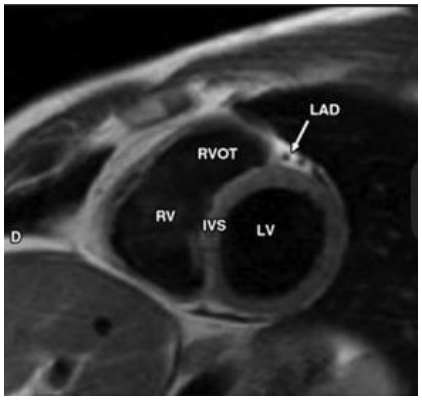

Figure 1:7 - Normal CMR anatomy shown in healthy subjects. IVS = interventricular septum, LAD = left anterior descending artery, LV = left ventricle, RVOT = left ventricular outflow tract, RV = right ventricle (17).

1.2.3 LV SEGMENTATION

The 17-segment American Heart Association (AHA) model (18) can be seen in Figure 1:8, to better understand the representation of myocardial segments. For regional analysis of the LV myocardium, the LV should be divided into equal thirds, perpendicular to the long axis of the heart, resulting in 3 circular basal, mid-cavity, and apical short-axis slices of the LV. The basal and mid-cavity slices should be divided into 6 segments of 60° each, as shown in Figure 1:8. (18)

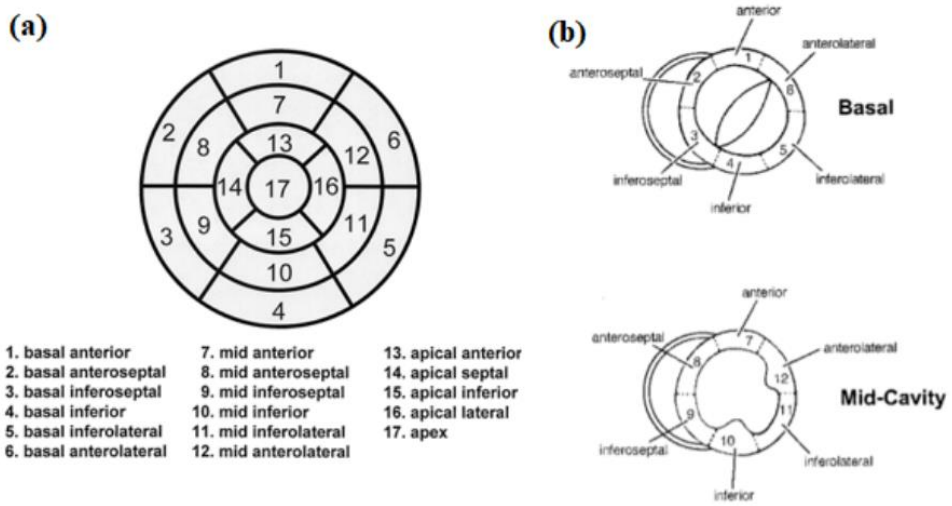

Figure 1:8 - LV Segmentation. a) Display of myocardial segments and the recommended nomenclature for tomographic imaging of the heart; b) Short-axis planes showing the name, location and anatomic landmarks for selection of the basal and mid-cavity short-axis slices (20)

1.2.4 LATE GADOLINIUM ENHANCEMENT

The cornerstone of CMR tissue characterization is the LGE which allows an optimal differentiation between normal and abnormal myocardium tissue after administration of gadolinium contrast.

LGE, often referred to as simply late enhancement (LE) imaging or delayed enhancement, has become a gold standard in myocardial viability assessment and provides an excellent depiction of myocardial infarction (MI) and macroscopic scarring. More recently, LE has played a broader role in the characterization of fibrosis in non-ischemic cardiomyopathies, and in the measurement of scar resulting from treatment. It's also used to diagnose and characterize a wide range of ischemic and non-ischemic cardiomyopathies such as HCM and myocarditis and has become pervasive in the CMR exam. (19)

Signal hyperintensities in LGE are observed in 60–70% of patients with HCM. (18) LGE has a high degree of accuracy and reproducibility in detecting focal regions of replacement fibrosis but is incapable of detecting diffuse interstitial fibrosis. (20) The contrast is visible after 7 minutes and until about 20 minutes after injection. The ratio of the distribution of these contrast agents in the tissue is different in healthy and diseased myocardium, accumulating in areas where there is extracellular space expansion, as in fibrosis. Tissues with increased volume of interstitial space also display slower extravasation rates as well as delayed re-absorption ("wash out") of contrast agent into the vascular space, this is why scarred tissue contains high concentrations of contrast agent compared to normal (viable) myocardium several minutes after bolus administration.

Therefore, Gadolinium Based Contrast Agents (GBCAs) are used for the detection and quantification of replacement fibrosis, since they shorten the T1 times of tissues where they accumulate. LGE images are usually generated using either magnitude reconstructed inversion recovery or Phase-Sensitive Inversion Recovery (PSIR) (21) techniques, that are acquired in a single-slice, single-breath-hold fashion, with multiple short-axis and long-axis (perpendicular to the short-axis) views. IR sequences are MRI sequences where radiofrequency pulses invert longitudinal magnetization, used to selectively null the signal for certain tissues - designed using the optimal inversion time to null the signal from the normal myocardium and maximize the contrast between normal myocardium and scar tissue. The healthy myocardium and post-infarct scar appear as black (suppression of the signal) and white, respectively, displaying a high contrast. Since there is suppression of the healthy myocardium signal, interstitial fibrosis will not be seen. Concluding, hyperintensity in LGE images is a marker of replacement fibrosis. (22)

1.2.5 T1 MAPPING

The T1 map consists of the formulation of a parametric map, which shows the value of the longitudinal relaxation time (T1) in milliseconds (ms) of each pixel in the region studied. The map is based on a series of images acquired at different times after an inversion-recovery radiofrequency pulse or 180º pulse, which inverts the hydrogen nuclei about the magnetic field. For it to be carried out perfectly, acquisitions must be made at identical times during different cardiac cycles, the equilibrium magnetization is either inverted or nulled with radiofrequency pulses, and T1-weighted images are acquired at

different times after the inversion time or time after application of the saturation pulse. (1,22)

Using these images, at different times after the initial radiofrequency pulse, we can measure the change in the signal intensity of the images and thus the time taken by the myocardial hydrogen nuclei to recover the signal. This is the longitudinal or T1 relaxation time of the myocardium.

T1 times depend on the tissue molecular properties and thus depend on the properties of the tissue. For example, regions with replacement fibrosis will appear as high-intensity signals on T1-weighted imaging.

Signals on T1-weighted imaging reflect variations in tissue composition, making T1 mapping a valuable technique for quantitative tissue characterization. Most MRI systems include a dedicated T1 mapping sequence known as the Look-Locker (LL) sequence, also referred to as the TI scout. However, the LL sequence is inherently influenced by heart rate variability and the timing of image acquisition within different phases of the cardiac cycle, which can introduce inconsistencies. Additionally, the delineation of epicardial and endocardial boundaries in T1 maps is subject to partial volume effects, potentially impacting the accuracy of myocardial tissue assessment.

The most widely validated T1 mapping method is the Modified Look-Locker Inversion Recovery (MOLLI) (23) pulse sequence that allows measurement of T1 times in a single breath-hold over 11 successive heartbeats. In protocol 5(3)3 MOLLI sequence, there is one inversion pulse with T1 sampling performed over 5 acquisition heartbeats, followed by 3 recovery heartbeats, and a second inversion pulse followed by 3 acquisition heartbeats. Variations of MOLLI have been proposed allowing shortened breath-hold durations. One example is the Shortened MOLLI (ShMOLLI) method, with a single breath-hold of only nine successive heartbeats. (22) In MOLLI sequences, T1 values need to be corrected by applying the following equation:

$$T1 = T1^{*} * \frac{B}{A - 1} \qquad (1.1)$$

The values of A, B, and T1 are estimated by curve-fitting using the three-parameter model.

An example of a T1 Mapping image used in this study is presented in Figure 1:9.

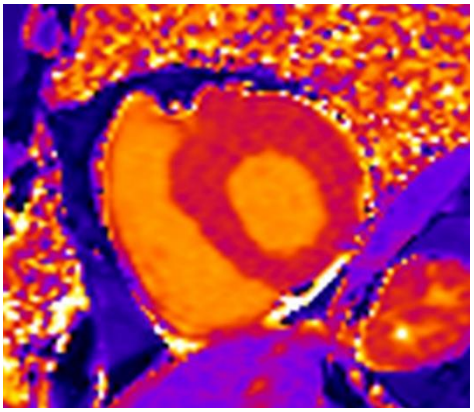

Figure 1:9 - T1 Mapping in a Healthy patient.

1.2.6 CINE IMAGING

CINE MRI is an imaging technique that captures the heart's motion throughout the cardiac cycle, presenting it in a continuous cine loop. Due to the high contrast between the myocardium and blood, it allows for clear visualization of dynamic changes in the cardiac chambers and ventricular walls, facilitating the assessment of ventricular function and regional wall motion. This technique is particularly useful for quantifying cardiac performance and identifying functional abnormalities. Modern CINE MRI primarily employs the balanced steady-state free precession (bSSFP) sequence, combined with retrospective ECG gating. The bSSFP sequence is a rapid gradient echo (GRE) technique in which the phase shift caused by imaging gradients is completely neutralized at each repetition time (TR), ensuring consistently high signal intensity even with very short TR values. Additionally, the unique T1/T2 contrast properties and inflow effects of bSSFP enhance the differentiation between myocardial tissue and blood. These advantages make CINE MRI highly accurate and reproducible, establishing it as a gold standard for evaluating left ventricular (LV) systolic function. Beyond volumetric quantification, CINE MRI provides valuable diagnostic insights when acquired in different imaging planes, including two-chamber, four-chamber, short-axis, and left ventricle/right ventricular inlet-outlet views. These acquisitions enable the evaluation of valvular insufficiency, outflow tract obstructions, ventricular dyssynchrony, and even the mobility of intracardiac masses or tumors. (24)

1.3 MYOCARDITIS

Myocarditis is an inflammatory disease of the myocardium, diagnosed by histological, immunological, and immunohistochemical criteria. When associated with cardiac

dysfunction (systolic or diastolic) it is classified as an Inflammatory Cardiomyopathy (ICM). (25)

CMR has emerged as a useful non-invasive imaging tool in the diagnostic work-up of patients with clinically suspected acute myocarditis (AM), where LGE and T2-weighted images are conventionally used to target the myocardial inflammatory process, including the presence of edema and necrosis/fibrosis. (3,26) While such CMR images are typically assessed qualitatively, CMR can also be deployed to collect quantitative information about the myocardial tissue properties. Parametric T1 and T2 mapping allows objective characterization of the regional distribution of AM in terms of the T1 and T2 relaxation times. However, their use in clinical routine has been limited because of the dependence on the chosen scanner and scan protocol, as well as on the patient's heart rate with a resulting overlap of T1 and T2 relaxation times between healthy and diseased tissue. (27–30) Thus, other imaging techniques that offer objective evaluation of patients with clinically suspected AM are desirable. (3)

In clinical practice, CINE imaging is used to provide morphological and functional information about the heart, focusing on the detection of ventricular dysfunction and pericardial effusion. (26) However, CINE images display a T2/T1-weighted contrast and should be able to capture active inflammatory processes and the development of fibrosis in the myocardium. In contrast to T2-weighted imaging, the CINE technique is known to be more robust and offers images of high fidelity.

An example of a myocarditis image is illustrated in Figure 1:10.

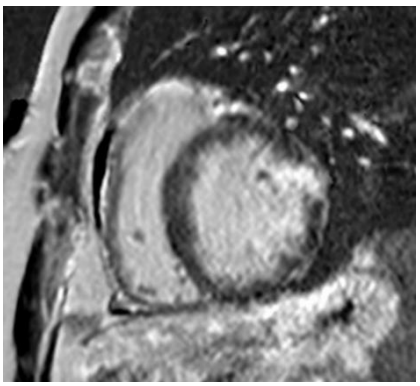

Figure 1:10 - Example of an LGE cardiac image, showing a myocarditis scar.

1.4 HYPERTROPHIC CARDIOMYOPATHY

HCM is most often caused by abnormal genes in the heart muscle. These genes cause the left ventricle (LV) walls to become thicker than normal. The thickened walls may become stiff and this can reduce the amount of blood taken in and pumped out to the body with each heartbeat, as is illustrated in Figure 1:11. (31)

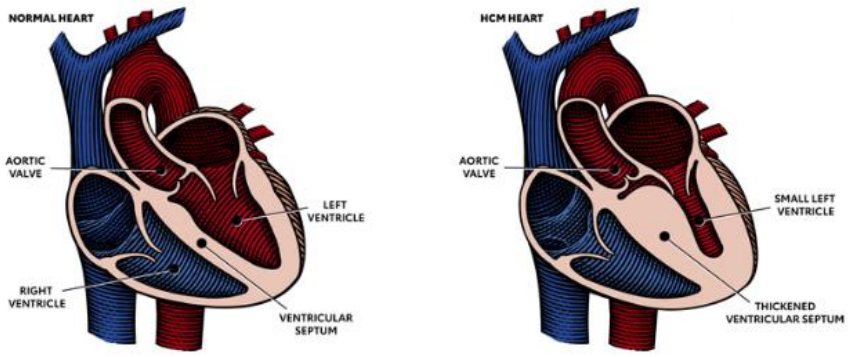

Figure 1:11 - On left is represented a normal myocardial heart and on right a HCM myocardial Heart representation (27).

In obstructive HCM, the thickened part of the heart muscle, usually the wall (septum) between the two ventricles, blocks or reduces the blood flow from the LV to the aorta. Two-thirds of the people with HCM have this type. In nonobstructive HCM, the heart muscle is thickened but doesn't block blood flow out of the heart. (31)

Some people with hypertrophic cardiomyopathy don't have symptoms while others may only feel symptoms with exercise or exertion. Some people may not have signs or symptoms in the early stages of the disease but may develop them over time. As HCM progresses, it can cause other health problems like a higher risk of developing atrial fibrillation, which can lead to blood clots, stroke, and other heart-related complications. HCM may also lead to heart failure and sudden cardiac arrest, but this is rare. It's estimated that as many as 1 in every 500 young people in the United States have HCM, but a large percentage of people are undiagnosed. This pathology is diagnosed based on medical history, family history, physical exam, and diagnostic test results of the patient. (31)

Identifying the patients with hypertrophic cardiomyopathy (HCM) in whom the risk of sudden cardiac death (SCD) justifies the implantation of a cardioverter-defibrillator (ICD) in primary prevention remains challenging. The European and American guidelines in

this setting use different risk stratification and criteria. A study performed by Pedro Freitas, António Miguel Ferreira, et al. (32), evaluated the role of CMR LGE in improving these risk stratification strategies and specifies that LGE has shown to be an independent predictor of SCD in HCM patients but is yet to be fully integrated into clinical decision algorithms. The article suggested that the amount of LGE has greater prognostic value than the two clinical risk stratification tools and their components. Using LGE for risk stratification would correctly reclassify a significant proportion of patients. However, the apparent superiority of LGE over clinical risk scores does not mean that these should be abandoned or replaced by this imaging marker. Instead, they believe that integrating clinical risk factors and the amount of LGE will probably yield the best results. A large and diverse population of HCM patients with comprehensive evaluation and long follow-up should be required to develop such a tool.

This pathology is presented in different patterns of myocardial fibrosis: interstitial diffuse fibrosis which, if not treated, evolves into replacement fibrosis. In the latest stage, there is a loss of myocardial properties. That´s why this study is so important.

An example of an LGE image of an HCM patient is illustrated in Figure 1:12.

Figure 1:12 - LGE image of a HCM patient

CHAPTER 2 METHODS AND STUDY DESCRIPTION

2.1 STUDY DESIGN

A retrospective study was carried out on images of patients undergoing cardiovascular examinations with the LGE, T1 Mapping, and CINE image sequences. The data was collected indirectly and manually by authorized health professionals. They were analyzed in a pseudo-anonymized way, recorded in a protected place only accessible to the study investigators, without compromising the right to confidentiality. All ethical principles of confidentiality and anonymity of the database were guaranteed. All ethical procedures in force at the host institution were respected. The images from each examination were exported, anonymized, and with no way of being traced, and only then sent for evaluation. Since it is a retrospective study, there was no possibility of changing what had already been done to the patients. All the patients gave their consent for their test to be used for research purposes.

The Ethics Committee of the Escola Superior de Tecnologia da Saúde de Lisboa (CE-ESTeSL) unanimously approved the issue of a favorable opinion, considering that the Clinical Research Committee of Hospital da Luz, by delegation of powers, ensured the authorization to carry out the study. The project was registered with number 50-2023 and it was approved on December 7, 2023.

2.2 STUDY SAMPLE

The sample consisted of 36 individuals with a clinical indication for cardiac magnetic resonance (CMR) examination due to myocarditis or hypertrophic cardiomyopathy (HCM). Among these, 18 individuals had a positive result for late gadolinium enhancement (LGE+) and 18 were considered healthy, as they showed no evidence of late gadolinium enhancement (LGE-) on the MRI images. The clinical indications included 27 patients with HCM (14 of whom were LGE+ and 13 LGE-) and 9 patients with myocarditis (4 of whom were LGE+ and 5 LGE-). An anamnesis was also carried out to collect demographic data on these individuals. They were recruited at Hospital da Luz Lisboa, where data collection was carried out, particularly in the Imaging service.

2.3 INCLUSION CRITERIA

The inclusion criteria were:

- Age over 18 years (inclusive)
- Availability of good quality LGE, T1 Mapping, and CINE images
- Suspicion/history of myocarditis or HCM
- Exams performed with 1.5T MRI

2.4 EXCLUSION CRITERIA

Exams that did not have sufficient image quality due to the presence of artifacts were excluded.

2.5 VARIABLES

The variables collected for this study are as follows:

- Demographic variables: age and sex;

- Continuous variables: means, standard deviations, and areas of the LGE+ ROIs and segments.

2.6 STUDY DESCRIPTION

The study was based on the selection of MRI scans of 18 individuals with medical confirmation of delayed enhancement and 18 individuals who did not have any areas with delayed enhancement presented. Both samples had a clinical indication for the examination of myocarditis or HCM. They were selected to understand the variation in signal intensity they showed in myocardial lesions, described as areas of hypersignal on MRI in the LGE sequences, compared to the CINE and T1 Mapping sequences, which are the sequences commonly used in this type of cardiac pathology to understand whether in LGE images the variation in signal intensity in the observed late enhancement areas will be similar in CINE and T1 Mapping images since this does not require contrast injection and could be a viable alternative for the patient CMR which contrast is not recommended.

2.6.1 IMAGE AQUISITION

This study was carried out in the Imaging department of Hospital da Luz, in Lisbon, as it had 1.5T MRI equipment, advanced image analysis workstations, advanced software for processing the acquired images, and a file system of digital images (PACS), in addition to the fact that the Imaging Service includes a specialist doctor with the title of Assistant, Doctor of Medicine (co-supervisor of this research and who suggested the topic covered). In addition to these aspects, the institution authorized the study to be carried out, given the interest shown in the possible results of this study.

All exams were carried out on the 1.5T MAGNETOM Sola Siemens scanner.

The acquisition protocol used was based on the standard protocol used in this institution (see Table 2:1.) below.

Table 2:1 - Sequences Parameters.

Sequence	T1 Mapping MOLLI	LGE	CINE_SAX
TR (ms)	263.9	653.0	33.1
TE (ms)	1.01	1.16	1.16
Bandwidth (Hz/pixel)	1085	1045	925
Slice Thickness (mm)	8.0	8.0	8.0
TI increment (ms)	180	280	
Flip Angle (º)	35	55	60
SNR	1.00	1.00	1.00
FOV (mm)	360	310	404
Sequence type	TRUFI	TRUFI	TRUFI
Voxel Size (mm3)	1.9x1.9x8.0	0.7x0.7x8.0	1.0x1.0x8.0

2.7 POST-PROCESSING

The images were processed using Circle's® software with cvi42's Cardiac MR which quantifies cardiac function, and flow and assesses tissue abnormalities faster with AI-based contouring. (33) In a total of three slices per patient LGE, T1 Mapping, and CINE images were visually evaluated for the presence of possible artifacts that would impair image quality. For the images that respected the chosen inclusion criteria, a first qualitative analysis was made to detect the presence/absence of hypersignal that would indicate late enhancement in the images.

2.7.1 PHASE I – LESION SEGMENTATION

To identify late enhancement in LGE images, the walls of the epicardium and endocardium of the LV myocardium in diastole were segmented semi-manually, using the available tool "PHASE AI LGE - Detect LV contours Current Phase" for a first segmentation and then, manual corrections and adjustments to the cardiac anatomy were performed. The segmentations performed were (See Fig. 2.1):

- ROI LV Endocardial contour (RED)
- ROI LV Epicardial Contour (GREEN)

Then, a reference region of interest (ROI) in the healthy myocardium (region with no contrast/hypersignal and with normal myocardial walls) was defined and drawn manually. The software defines the regions with late enhancement as being the areas

with an intensity 6SD higher than the normal ROI. These areas appear in a yellowish color and a ROI including all that area was drawn and is defined as the LGE+ zone (see Figure 2:1).

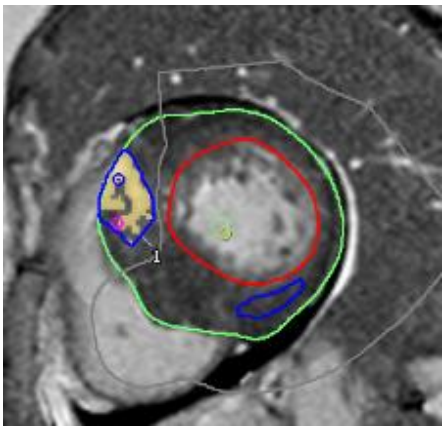

Figure 2:1 – LGE sequence with the ROI of reference and ROI of LGE+ drawn.

The traditional 6 SD method was chosen according to previous studies (21,34–36) and treats each pixel as dichotomously diseased or not diseased (healthy/unhealthy), if the signal intensity is, respectively, higher or lower than the cut-off value.

That said, the 6SD threshold was used in the segmentation of delayed enhancement areas in this study and, to guarantee the veracity of the results, all enhancement areas generated with this method were overall checked by the doctor available at the service.

For this study, patients, ROIs, and Segments with positive late enhancement are referred to as LGE+ and without late enhancement as LGE-.

2.7.2 PHASE II – MYOCARDIUM SEGMENTS DELIMITATION

After completing the lesion segmentation process, a segmentation of the myocardium was performed to better understand the variation of intensities in each segment. For that purpose, the myocardium was divided into 4 sections, because that was considered easier to reproduce in all patients, instead of 6, as suggested by the American Heart Association for LV segmentation of middle slices (Figure 1.8). A diagonal line was drawn that divides the septal wall in the middle and intercepts the RV vertex. Then a perpendicular wall was drawn that connects to the upper RV/LV interception point (Figure 2:2 a)).

Then, a ROI was manually drawn between the epicardial and endocardial lines for each segment. The final myocardial segments represented in Figure 2:2 b), are the result of

the intersection of these ROIs. Due to the different image's orientations and sizes of each patient's heart, these sections were manually drawn for each subject, always with attention to their boundaries so that they didn't overlap and so that there was no contact with the LV and RV.

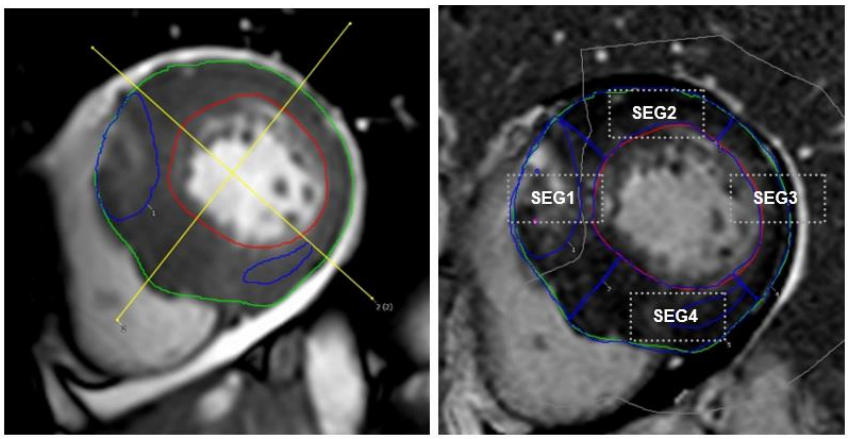

Figure 2:2 – CINE and LGE images for the same LGE+ patient; a) Segmentation process in CINE image of an LGE+ patient. b) Final result of manual segmentation of the myocardium and labeling in LGE image for LGE+ patient.

2.7.3 PHASE III – REPRODUCE ROIS

After phase II, all the aforementioned ROIs (LGE+ ROI and the 4 segment ROIs) were copied and pasted exactly in the same position and with the same approximate dimension in T1 and CINE imaging techniques.

2.7.4 PHASE IV – EXTRACTING QUANTITATIVE DATA

For each patient and for each slice selected from the 3 sequences, the following values were taken:

1. Mean + standard deviation (SD) of the LGE+ ROIs and of each segment.
2. areas of all ROIs

2.7.5 PHASE V – "BLIND TEST" AND EXTERNAL VALIDATION

In this final phase, cases of CINE and T1 Mapping were randomly selected (LGE+ and LGE-). Subsequently, these cases were presented, without ROIs and without access to the LGE images, to an experienced doctor, to see if he would be able to observe areas of hypersignal in the LGE+ cases without access to the LGE images.

2.8 IMAGE ANALYSIS

The quality of the images analyzed were assessed by an experienced reader. Each original image was evaluated for artifacts and the presence of any type of artifact led to their exclusion from the study.

For qualitative analysis, this was done in a general way, considering the areas of enhancement shown on the LGE and also recording the segments with hypersignal and which were positive in Phase I of the study.

For the quantitative analysis, since the T1 Mapping and CINE images can't be directly compared, as one has fixed values associated with it (T1 Mapping) and the other has variable values from patient to patient (CINE), an analysis was first made of the T1 Mapping considering the value of 1045ms (defined by the hospital and physician present in the study) as the maximum value for a healthy myocardium, so that above this value the patients were considered positive for enhancement (LGE+), making an analysis by segment and by enhancement ROI copied from our LGE image. Next, the process is similar in the CINE, but as no established reference value for normal myocardium is available, a weighted average of the segments considered healthy in the LGE image was performed and used as a reference.

2.9 STATISTICAL ANALYSIS

Baseline characteristics will be shown as means and standard deviation (SD). The values obtained from T1 will be displayed as mean values in ms and in CINE are presented as mean values of intensity and percentages. For both, the specificity, precision, sensibility and accuracy were calculated.

The procedure explained above will then be applied to one slice per patient, per sequence (CINE and T1Mapping), i.e. 2 images per patient will be taken, out of the 18 available, and the 4 myocardial segments and LGE+ ROI will be measured.

Demographic data and technical data on the acquisition of the exam and its outcome after processing the acquired images were collected on a sheet specifically designed for this purpose in Excel format. The XLMiner Analysis ToolPak add-in for Microsoft Excel 365 was used for data processing. Continuous variables are presented as means and standard deviation and categorical variables as percentages.

The fundamental measures of diagnostic accuracy are sensitivity (i.e., true positive rate (TPR)) and specificity (i.e., true negative rate (TNR)). Sensitivity quantifies the proportion of actual positive cases that a test correctly identifies, indicating how effectively it detects the condition being evaluated (see Equation 2.1). A highly sensitive model will flag almost everyone who has the disease and not generate many false-negative results. Specificity measures the ability of a model to correctly generate a negative result for people who do not have the condition under test (see Equation 2.2). A high-specificity test will correctly

rule out almost everyone who does not have the disease and will not generate many false-positive results. In the following equations, TP = True Positive, TN = True Negative, FP = False Positive and FN = False Negative (37).

$$Sensitivity = \frac{TP}{TP+FN} \qquad (2.1)$$

$$Specificity = \frac{TN}{TN+FP} \qquad (2.2)$$

Accuracy measures how close a given set of observations is to their true value (see equation 2.3).

Precision measures how close the observations are to each other, and this will also be calculated based on the data (see Equation 2.4).

$$Accuracy = \frac{TP+TN}{TN+FN+TP+FP} \qquad (2.3)$$

$$Precision = \frac{TP}{TP+FP} \qquad (2.4)$$

CHAPTER 3 RESULTS

This chapter will present the results of the analysis described in points 2.8 and 2.9.

3.1 SAMPLE DEMOGRAPHICS

This study was based on 18 individuals considered healthy (LGE-), i.e. without late enhancement on LGE images, and 18 individuals with enhancement (LGE+) on LGE. The characteristics of the sample studied are shown in Table 3:1.).

Table 3:1 - Description of the study sample. The values for age are presented as means ± standard deviations. The values for sex are presented as the number and percentage of females.

	LGE -	LGE +	p-value
Age	52.9 ± 17.5	54.6 ± 16.6	0.78
Sex (F) (%)	6 (33%)	6 (33%)	-

A two-sample t-test with equal variances was carried out to compare the mean ages of the two groups of patients, and no significant difference was observed between them.

3.2 QUALITATIVE ANALYSIS

3.2.1 Qualitative comparative analysis of the LGE, CINE, and T1 images

After visually inspecting the CINE images and T1 maps for each patient (see appendix 1), TP, FP, TN and FN were determined, and specificity, accuracy, precision sensitivity were calculated.

Table 3:2 - Results of initial qualitative analysis of the sequences in LGE+ and LGE- patients.

	TP	TN	FP	FN	SENSITIVITY	SPECIFICITY	PRECISION	ACCURACY
T1	10	15	3	7	0.588	0.833	0.714	0.769
CINE	12	18	0	6	0.667	1	0.833	1

From the results presented in Table 3:2, both T1 Mapping and CINE images have a low sensitivity, which means that, from the outset, both imaging techniques have difficulty in detecting most of the TP cases (less than 70%). However, regarding specificity, T1 Mapping proved to be better detecting healthy cases than pathology, detecting around 83% of the TN cases and CINE proved to be 100% effective in detecting healthy individuals, as all negative cases were correctly identified.

Finally, considering the precision and accuracy of both images, CINE showed greater results, showing a high ability to correctly detect the overall cases and the ones with disease. So, the qualitative analysis has shown that CINE images are more precise and accurate compared to T1 Mapping.

3.3 QUANTITATIVE ANALYSIS

3.3.1 Quantitative comparative analysis of T1 maps and LGE+ ROIs in patients with disease

First, the regions of LE were identified in the LGE images. These regions of interest (ROIs) were then copied to the T1 maps to verify whether the hypersignal was also detectable in those images. The mean value of the ROIs in the T1 maps was calculated and registered (see appendix 2), and if it was higher than the reference value (1045 ms), the region was considered to have hypersignal. Then, two analyses were performed:

In the analysis T1 ROI-1, the following definitions were considered:

- **TP** - Value above 1045 ms in at least one ROI and in agreement with LGE
- **TN** - Value below 1045 ms in at least one ROI and in agreement with LGE
- **FP** - Value above 1045 ms in at least one ROI and not in agreement with LGE
- **FN** - Value below 1045 ms in at least one ROI and not in agreement with LGE

In the analysis T1 ROI-2, the following definitions were considered:

- **TP** - Value above 1045 ms in all ROIs and in agreement with LGE
- **TN** - Value below 1045 ms in all ROIs and in agreement with LGE
- **FP** - Value above 1045 ms in all ROIs and not in agreement with LGE
- **FN** - Value below 1045 ms in all ROIs and not in agreement with LGE

The results obtained are summarized in Table 3:3.

Table 3:3 - Results of ROI analysis in T1 mapping images.

	TP	TN	FP	FN	SENSITIVITY	PRECISION
T1 ROI-1	15	0	0	2	0.882	1
T1 ROI-2	14	0	0	3	0.824	1

From the results presented in Table 3:3, it is seen that, the T1 Mapping images have a sensitivity of 88% to detect at least one ROI of LE. This means that 88% of the cases with disease were correctly detected using T1 images. Considering the precision of both analyses, it also demonstrated a 100% in the results presented, which means that all the cases detected with disease were correct.

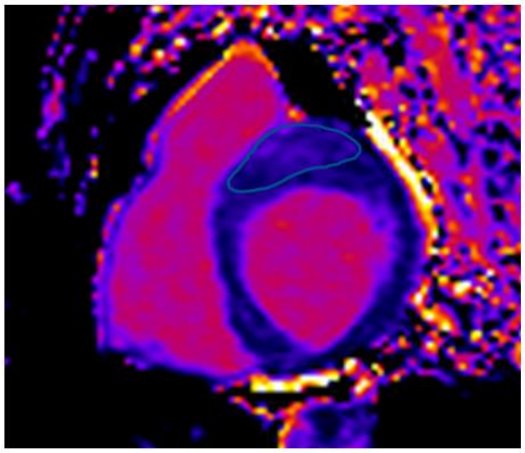

Figure 3:1 - Representation of a T1 Mapping LGE+ patient, and his ROI.

3.3.2 Quantitative comparative analysis of T1 maps and LGE images per segment in patients with disease

Analyzing the 4 segments delineated in the LGE images per diseased patient, were observed in 18 LGE+ patients (72 segments analyzed in total) were identified 29 positive segments, the majority were in Segment 1 (40,3%), 8 patients had more than one LGE+ segment presented, and 3 patients had more than one ROI of LGE+ (see appendix 3).

A broader analysis was then carried out, comparing the segments, to understand whether there would be any differences in the detection of disease between the segments. The advantage of this analysis is that it does not require the delineation of a ROI of the enhanced region.

The following definitions were considered for the analysis:

- **TP** - Value above 1045 ms in the segment and in agreement with LGE
- **TN** - Value below 1045 ms in the segment and in agreement with LGE
- **FP** - Value above 1045 ms in the segment and not in agreement with LGE
- **FN** - Value below 1045 ms in the segment and not in agreement with LGE

Table 3:4 - Results of the analysis by Segments in T1 Mapping images, in LGE+ Patient.

SEGMENT 1								
	TP	**TN**	**FP**	**FN**	**SENSITIVITY**	**SPECIFICITY**	**ACCURACY**	**PRECISION**
T1	11	3	4	0	1	0.429	0.778	0.733
SEGMENT 2								
	TP	**TN**	**FP**	**FN**	**SENSITIVITY**	**SPECIFICITY**	**ACCURACY**	**PRECISION**
T1	2	7	5	4	0.333	0.583	0.5	0.286
SEGMENT 3								
	TP	**TN**	**FP**	**FN**	**SENSITIVITY**	**SPECIFICITY**	**ACCURACY**	**PRECISION**
T1	2	11	3	2	0.5	0.786	0.722	0.4
SEGMENT 4								
	TP	**TN**	**FP**	**FN**	**SENSITIVITY**	**SPECIFICITY**	**ACCURACY**	**PRECISION**
T1	6	5	6	1	0.857	0.455	0.611	0.5

So, in this analysis, there are already some important differences to mention. In the case of Segment 1, which was the segment with the highest incidence of LGE+ areas, shows an excellent sensitivity, as all cases that had enhancement in this segment were properly identified. Still, observing its specificity we obtained a very low value (43%) since the cases that would be expected to be negative, in this method failed in their detection. Considering the precision and accuracy, it demonstrated good values in the results presented (73% and 78%, respectively), which means that the method for segment 1 was good at detecting cases correctly, with or without disease present.

For segment 2, all values obtained were reduced. Therefore, for this segment, the method did not prove to be effective in detecting the disease, being the segment that showed the worst accuracy in the analysis, as well as the cases in general, both negative and positive, since its accuracy and specificity were also greatly reduced.

In segment 3, a higher specificity value was obtained (78%). However, the cases in which values greater than 1045 ms should have been detected, that is, within this segment, decreased, having only 50% sensitivity and precision of 40%, influenced by this same reason. However, the accuracy shown was considered good (72%), influenced by the TN that the method presented.

Finally, in segment 4, sensitivity was also high (86%) as we had a greater number of TPs identified. In this segment, the specificity and precision dropped, and the accuracy was not the best, showing us that, in this method, the segment only was right in 61% of the cases.

In general, we consider that the results from segment 1 were more accurate, reaching almost 80%, sensitive for detecting pathology, but in terms of specificity, segment 3 was better. The fact that there are more enhanced areas in Segment 1 may also have influenced this analysis.

3.3.3 Quantitative comparative analysis of CINE images and LGE+ ROIs in patients with disease

A similar analysis to the one performed on the T1 maps was carried out in the CINE images, where the mean values taken from the LE ROIs were compared with a reference value (see appendix 4 and 5). This reference value was estimated by calculating the weighted average of the CINE images segments that were considered LGE- in the LGE images. Due to the variation of signal intensity intrinsic to the CINE images, the reference value has to be calculated for each patient.

In the analysis CINE ROI-1, the following definitions were considered:

- **TP** - Value above the reference in at least one ROI and in agreement with LGE
- **TN** - Value below the reference in at least one ROI and in agreement with LGE
- **FP** - Value above the reference in at least one ROI and not in agreement with LGE
- **FN** - Value below the reference in at least one ROI and not in agreement with LGE

In the analysis CINE ROI-2, the following definitions were considered:

- **TP** - Value above the reference in all ROIs and in agreement with LGE
- **TN** - Value below the reference in all ROIs and in agreement with LGE
- **FP** - Value above the reference in all ROIs and not in agreement with LGE
- **FN** - Value below the reference in all ROIs and not in agreement with LGE

The results can be seen in Table 3:6.

Table 3:5 - Results of ROI analysis in CINE images, in LGE+ patients.

	TP	TN	FP	FN	SENSITIVITY	PRECISION
CINE ROI - 1	13	0	0	5	0.722	1
CINE ROI -2	10	0	0	8	0.556	1

From the results presented in Table 3:7, it is seen that the CINE images have a sensitivity of 72% to detect at least one ROI of LE. This means that 72% of the cases with the disease were correctly detected using CINE images. Considering the precision of both analyses, it also demonstrated excellent precision in detecting disease by ROI.

However, as much as we want to be more sensitive to the identified areas, we lose sensitivity with CINE images, only being completely correct in LGE+ ROIs in 56% of cases.

In figure 3:2 an illustration of two patients with the disease and the ROIs delimitated are shown.

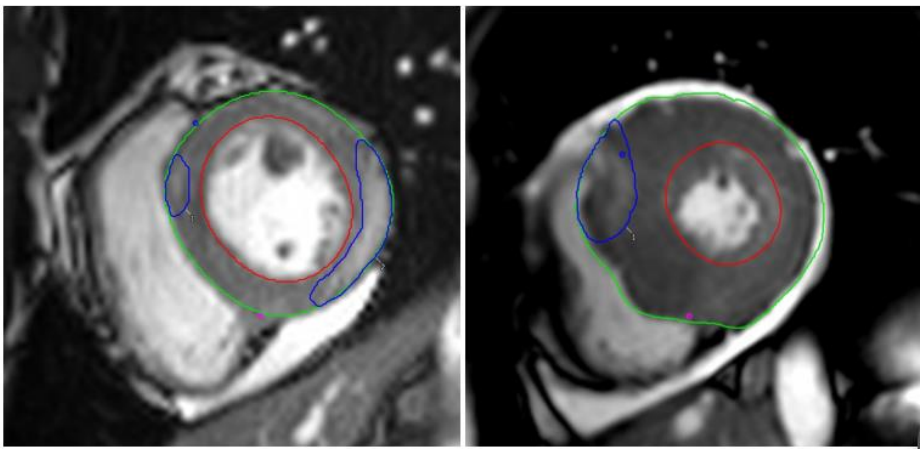

Figure 3:2 - CINE Images in LGE+ patients and their ROIs. On the left we can see a patient with 2 ROIs drawn, and on right a patient with one ROI.

3.3.4 Quantitative comparative analysis of CINE and LGE images per segment in patients with disease

Comparably with what was done in T1 Mapping images, an analysis by segments was performed, for each patient. This analysis was carried out considering the reference average previously calculated for the analysis by ROIs, comparing it with the average of each segment. The results are presented in Table 3:8.

In the Analysis I, the following definitions were considered:

- **TP** - Value above reference in at least one of the segments and in agreement with LGE

- **TN** - Value below reference in at least one of the segments and in agreement with LGE
- **FP** - Value above reference in at least one of the segments and not in agreement with LGE
- **FN** - Value below reference in at least one of the segments and not in agreement with LGE

In the Analysis II, the following definitions were considered:

- **TP** - Value above reference in segments and in total agreement with LGE
- **TN** - Value below reference in segments and in total agreement with LGE
- **FP** - Value above reference in segments and not in total agreement with LGE
- **FN** - Value below reference in segments and not in total agreement with LGE

Table 3:6 - Results of the two analyses performed in CINE images, by segments, for LGE+ patients.

CINE	TP	TN	FP	FN	SENSITIVITY	PRECISION
Analysis I	13	0	0	5	0.722	1
	TP	**TN**	**FP**	**FN**	**SENSITIVITY**	**PRECISION**
Analysis II	11	0	0	7	0.611	1

Observing analyses I and II on the CINE images, better results were obtained, with a sensitivity of 72% for analysis I in identifying correctly the segments with LE, and in analysis II we realized that they did not lose a lot of sensitivity, decreasing only 11% (the equivalent of 2 failed TP cases). The precision in this method for CINE was also 100%.

In figure 3:3 a representation of a CINE image segmented are shown.

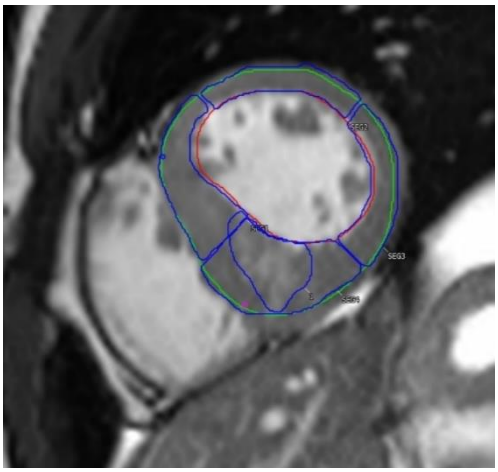

Figure 3:3 - CINE Image in LGE+ patients, segmented in 4 segments.

3.4 EXTERNAL VALIDATION

3.4.1 "Blind" visual analysis to check for agreement with the results presented

In this qualitative test, as described in point 2.7.5, 14 LGE- and 16 LGE+ patients were randomly selected and visually evaluated by the physician, with the order of presentation being random and completely "blind". As was done in the quantitative analyses, in this test the physician also indicated which segments he considered to have lesions (see Appendix 6). The results from these two analyses are presented in Table 3:8.

In Analysis I, the following were considered:

- **TP** - Visual identification of LE in at least one segment and in agreement with LGE
- **TN** – Not identify LE and in agreement with LGE
- **FP** - Visual identification of LE In at least one segment and not in agreement with LGE
- **FN** - Not identify LE and not in agreement with LGE

In Analysis II, the following were considered:

- **TP** - Visual identification of LE in all the segments in agreement with LGE
- **TN** – Not identify LE and in agreement with LGE
- **FP** - Visual identification of LE and not in agreement with LGE
- **FN** - Not identify LE and not in agreement with LGE

Table 3:7 - Results of Blind test analysis for validation of results, in CINE and T1 Mapping images.

	Analysis I							
	TP	**TN**	**FP**	**FN**	**SENSITIVITY**	**SPECIFICITY**	**ACCURACY**	**PRECISION**
T1	11	11	3	5	0.688	0.688	0.733	0.786
CINE	12	12	3	4	0.75	0.75	0.774	0.8
	Analysis II							
	TP	**TN**	**FP**	**FN**	**SENSITIVITY**	**SPECIFICITY**	**ACCURACY**	**PRECISION**
T1	7	11	3	9	0.438	0.55	0.6	0.7
CINE	7	11	3	9	0.438	0.55	0.6	0.7

As a result of this test, relevant conclusions can be taken for this study.

In analysis I, in T1 Mapping images, the physician identified pathology correctly in 69% of the cases and almost all that did not have disease present, with a specificity of 69%.

In the CINE images, slightly higher values were obtained. Through overall visual analysis, the physician was able to identify 75% of the pathology regions presented and obtained a specificity of 75%. The accuracy and precision for both images obtained values above 70% and very close to each other, which is considered a good result, meaning that the physician was able to identify diseased and healthy patients only with access to T1 Mapping and CINE images.

In analysis II, a decrease in the sensitivity was observed, since in both images there was a reduction in the percentage of TP present the physician couldn't detect disease in exactly all the segments where it was present. In addition, the accuracy and precision also decreased. This method has shown us that it is possible to perceive signal variations in the images and tell whether there is disease present and can do so accurately. However, in most cases, it may fail to detect the exact segment it is in because it is less sensitive in both images.

A final analysis was carried out to see how many cases the physician was able to identify the existence of enhancement in at least one of the two images (T1 mapping and CINE).

In this analysis, the following were considered:

- **TP** - Visual identification of LE in at least one modality T1Map/CINE and agreement with LGE
- **TN** – Not identify LE in neither of the sequences and agreement with LGE
- **FP** - Visual identification of LE in at least one modality T1Map/CINE and not in agreement with LGE
- **FN** - Not identify LE in neither of the sequences and not in agreement with LGE

Table 3:8 - Results of Blind test analysis for validation of results, per patient.

TP	TN	FP	FN	SENSITIVITY	SPECIFICITY	ACCURACY	PRECISION
14	10	4	2	0.875	0.833	0.8	0.778

Looking at the results of this analysis, the sensitivity, specificity, and accuracy were over 80%, which is considered a very good result, and the precision was not far off either, at 78%. This means that in 88% of the cases the physician was able to visually detect the pathology in at least one of the images, and in 83% of the cases identified correctly the absence of disease.

CHAPTER 4 DISCUSSION/CONCLUSIONS

In this study, which included 18 patients with LGE+ and 18 LGE-, 29 positive segments were identified, with the highest incidence in Segment 1 (40.3%). It was observed that both T1 Mapping and CINE images had limitations in detecting diseased segments. In an initial visual test T1 Mapping images had a sensitivity of less than 70% in identifying truly positive cases but showed good specificity (83%). In contrast, CINE images achieved 100% specificity in identifying healthy individuals and were more precise and accurate in detecting pathologies. However, a disadvantage of this initial assessment is that the possible areas of enhancement in the images are already known in advance.

Analysis by segment revealed that T1 Mapping showed variations in sensitivity and accuracy. In Segment 1, a high value for sensitivity was obtained. The results for this specific segment were expected to perform better, since it is more likely to have enhancement and is denser, as it is the segment most frequently affected in HCM and therefore with fibrosis. So, this variation of the signal should be entirely (or almost entirely) explained by the different prevalence and intensity of the disease, and not because it is more difficult to detect in different segments of the image. This decrease of specificity could be solved in at least many cases if it were done on a computer and not by ROIs, which could have been done with ML. Results in Segments 2 and 3 showed a significant drop in accuracy and sensitivity, while in Segment 4 results showed high sensitivity (86%) but reduced accuracy (61%). On the other hand, the CINE images showed greater consistency, with 72% sensitivity in detecting areas with LE, and better overall performance in correctly identifying the affected segments. It would have been interesting if the reference value used in the CINE images had been normalized in the analysis, but that was not possible due to the variation between images from patient to patient. Perhaps with a larger sample there could have been this possibility.

It's important to mention some kind of limitation in the 6SD method used to detect LGE areas, is that there is a need to identify regions of presumed healthy myocardium to provide the necessary contrast between affected and unaffected tissues. If these regions are available, their identification by the user introduces subjectivity to the analysis. Conversely, if they are not present, diffuse fibrosis can go undetected with LGE. Moreover, is a semi-quantitative technique: late enhancement is either present or not.

Our main objective was to find out whether it was possible to use CINE and/or T1 Mapping as the first triage to detect possible candidates for LGE scans. Ideally, it would be enough for the physician not to detect a hypersignal in any of the modalities (CINE

and/or T1 Mapping) for the patient to be considered negative and, consequently, released from undergoing the exam in which contrast is injected.

Through the performed blind analysis, it was found that in 75% of the patients the physician didn't identify a lesion and they really were negative patients, which means that through this method, these 75% of patients would not need to inject contrast and only failed in 25% of them.

Analyzing the results obtained per patient including both modalities, it was found that the physician was correct in 87.5% of the positive cases, identifying at least one of the hypersignal modalities, which would mean that these 87.5% would go on to inject contrast and with only 12.5% not going to. On the other hand, it would be possible to exclude 83% of patients from contrast injection, as the physician was able to identify that there was no enhancement in any of the modalities, failing only 17% of cases.

These results are considered very positive since, with this first triage, it would be possible to exclude a large number of patients considered healthy from undergoing contrast examinations, being advantageous concerning the risks associated, known and unknown, with the injection of gadolinium contrast. It would also reduce expenses (more economical), increase the profitability of the service (more patients on the same machine and more exams carried out in less time) and it would be important when there is no gadolinium available (as happened during the COVID period) as these types of exams could still be carried out.

Through the quantitative analysis, it is also possible to understand the usefulness and importance of developing ML software to detect differences in signal intensity more accurately.

Additionally, future improvements could include increasing the number of LGE+ patients to increase the sensitivity of the techniques and considering T2 Mapping analysis, particularly useful in cases of myocarditis. An interesting point of exploration would be to investigate signal variations in CINE images during systole and diastole, since in some cases, the hypersignal was more evident in systole.

Recent studies also suggest the use of ML algorithms for automatic lesion detection based on non-contrast images, such as CINE. Training networks with data from all modalities (LGE, CINE, T1, and T2 Mapping) can allow for the automatic extraction of information, potentially allowing for the accurate identification of enhancement areas, even in the absence of the LGE sequence. Thus, new approaches such as radiomics

analysis and ML have the potential to significantly improve clinical practice and reduce costs and examination time.

The study by C. Neves Silvestre Baleia et al. (22) suggests that it is possible to carry out a quantitative assessment of fibrosis in a more accessible and safer way, avoiding the use of gadolinium contrast, which can cause complications for some patients. Another relevant point was the concept of Native Virtual Enhancement (NVE), which transforms native T1 maps into images like LGE, potentially revolutionizing clinical practice by reducing the time and cost of exams.

In parallel, the study by E. Avard, I. Shiri, G. Hajianfar, et al. (38) explored the use of ML to identify myocardial infarction in non-contrast Cine-CMR images, demonstrating high diagnostic accuracy. On the other hand, H. Wang, Y. Chen, C. Ma et al. (39) proposed the use of ML with complete and absent modalities to train networks with data from multiple image sequences (LGE, CINE, T1 and T2 Mapping), investigating the possibility of identifying areas of enhancement without depending on the LGE sequence.

These studies reinforce the potential of non-contrast and ML techniques to replace or complement LGE, promoting safer and more efficient diagnoses in the future.

CHAPTER 5 BIBLIOGRAPHIC REFERENCES

1. Filipa A, Soares P. INSTITUTO POLITÉCNICO DE LISBOA ESCOLA SUPERIOR DE TECNOLOGIA DA SAÚDE DE LISBOA OTIMIZAÇÃO DE UM NOMOGRAMA T1 E T2 MAPPING MIOCÁRDICO ORIENTADOR: PROFESSORA DOUTORA MARIA MARGARIDA RIBEIRO-Professora Adjunta da Escola Superior de Tecnologia da Saúde de L.

2. Elsafty HG, El Shafey M, El Arabawy R, Mahrous MR, Dawoud TM. Could native T1 mapping replace late gadolinium enhancement in the assessment of myocardial fibrosis in patients with cardiomyopathy? Egypt J Radiol Nucl Med [Internet]. 2021 Dec 1 [cited 2023 Jul 5];52(1):1–11. Available from: https://link.springer.com/articles/10.1186/s43055-021-00520-2

3. Papalini EI, Polte CL, Bobbio E, Lagerstrand KM. Diagnosis of Acute Myocarditis Using Texture-Based Cardiac Magnetic Resonance, with CINE Imaging as a Novel Tissue Characterization Technique. Diagnostics [Internet]. 2022 Dec 1 [cited 2024 Sep 3];12(12). Available from: /pmc/articles/PMC9777125/

4. Collidge TA, Thomson PC, Mark PB, Traynor JP, Jardine AG, Morris STW, et al. Gadolinium-enhanced MR imaging and nephrogenic systemic fibrosis: retrospective study of a renal replacement therapy cohort. Radiology [Internet]. 2007 Oct [cited 2024 Sep 3];245(1):168–75. Available from: https://pubmed.ncbi.nlm.nih.gov/17704357/

5. Magnetic Resonance Imaging (MRI) [Internet]. [cited 2024 Aug 14]. Available from: https://www.nibib.nih.gov/science-education/science-topics/magnetic-resonance-imaging-mri

6. Rodgers CT, Robson MD. Cardiovascular magnetic resonance: physics and terminology. Prog Cardiovasc Dis [Internet]. 2011 Nov [cited 2024 Aug 14];54(3):181–90. Available from: https://pubmed.ncbi.nlm.nih.gov/22014486/

7. Ridgway JP. Cardiovascular magnetic resonance physics for clinicians: Part i. J Cardiovasc Magn Reson [Internet]. 2010 Nov 30 [cited 2024 Aug 14];12(1):1–28. Available from: https://jcmr-online.biomedcentral.com/articles/10.1186/1532-429X-12-71

8. Murphy A, Ballinger J. MRI pulse sequences. Radiopaedia.org [Internet]. 2013 Mar 1 [cited 2024 Aug 16]; Available from: http://radiopaedia.org/articles/21957

9. Belloni E, De Cobelli F, Esposito A, Mellone R, Perseghin G, Canu T, et al. MRI

of cardiomyopathy. Am J Roentgenol [Internet]. 2008 Dec 23 [cited 2024 Aug 16];191(6):1702–10. Available from: https://www.ajronline.org/doi/10.2214/AJR.07.3997

10. Filipa A, Soares P. Otimização de um nomograma T1 e T2 mapping miocárdico. 2020 [cited 2024 Aug 14]; Available from: https://repositorio.ipl.pt/handle/10400.21/13879

11. Weerakkody Y. TRUFI sequence. Radiopaedia.org [Internet]. 2023 Aug 21 [cited 2024 Aug 27]; Available from: https://radiopaedia.org/articles/trufi-sequence

12. Mahrholdt H, Wagner A, Judd RM, Sechtem U, Kim RJ. Delayed enhancement cardiovascular magnetic resonance assessment of non-ischaemic cardiomyopathies. Eur Heart J [Internet]. 2005 Aug [cited 2023 Jul 4];26(15):1461–74. Available from: https://pubmed.ncbi.nlm.nih.gov/15831557/

13. Anatomy and Physiology of the Heart - Normal Function of the Heart - Cardiology Teaching Package - Practice Learning - Division of Nursing - The University of Nottingham [Internet]. [cited 2024 Aug 27]. Available from: https://www.nottingham.ac.uk/nursing/practice/resources/cardiology/function/anatomy.php

14. Tran DB, Weber C, Lopez RA. Anatomy, Thorax, Heart Muscles. StatPearls [Internet]. 2024 Jun 22 [cited 2024 Aug 27]; Available from: https://www.ncbi.nlm.nih.gov/books/NBK545195/

15. Ginat DT, Fong MW, Tuttle DJ, Hobbs SK, Vyas RC. Cardiac imaging: Part 1, MR pulse sequences, imaging planes, and basic anatomy. Am J Roentgenol [Internet]. 2011 Oct 23 [cited 2024 Sep 8];197(4):808–15. Available from: https://www.ajronline.org/doi/10.2214/AJR.10.7231

16. Ginat DT, Fong MW, Tuttle DJ, Hobbs SK, Vyas RC. Cardiac imaging: Part 1, MR pulse sequences, imaging planes, and basic anatomy. Am J Roentgenol [Internet]. 2011 Oct 23 [cited 2024 Aug 27];197(4):808–15. Available from: https://ajronline.org/doi/10.2214/AJR.10.7231

17. Nacif MS, De Oliveira AC, Carvalho ACP, Rochitte CE. Ressonância magnética cardíaca e seus planos anatômicos: como eu faço? Arq Bras Cardiol [Internet]. 2010 [cited 2024 Sep 8];95(6):756–63. Available from: https://www.scielo.br/j/abc/a/XBcqdWv64pDTgBXyRPKytdr/

18. Lyons KS, Dixon LJ, Johnston N, Noad R, Hamilton A, McKeag N, et al. Late gadolinium enhancement is common in patients with hypertrophic cardiomyopathy and no clinical risk factors for sudden cardiac death: A single center experience. Cardiol J [Internet]. 2014 [cited 2024 Sep 8];21(1):29–32. Available from: https://pubmed.ncbi.nlm.nih.gov/23990187/

19. Kellman P, Arai AE. Cardiac Imaging Techniques for Physicians: Late Enhancement. J Magn Reson Imaging [Internet]. 2012 Sep [cited 2024 Sep 8];36(3):529. Available from: /pmc/articles/PMC3428749/

20. Mentias A, Raeisi-Giglou P, Smedira NG, Feng K, Sato K, Wazni O, et al. Late Gadolinium Enhancement in Patients With Hypertrophic Cardiomyopathy and Preserved Systolic Function. J Am Coll Cardiol [Internet]. 2018 Aug 21 [cited 2024 Sep 8];72(8):857–70. Available from: https://pubmed.ncbi.nlm.nih.gov/30115224/

21. Spiewak M, Malek LA, Misko J, Chojnowska L, Milosz B, Klopotowski M, et al. Comparison of different quantification methods of late gadolinium enhancement in patients with hypertrophic cardiomyopathy. Eur J Radiol [Internet]. 2010 Jun [cited 2024 Sep 8];74(3). Available from: https://pubmed.ncbi.nlm.nih.gov/19523780/

22. Neves Silvestre Baleia C, Raquel Conceição P, Rita Nunes P, Superior Técnico I. Comparison of T1-maps and Late Gadolinium Enhancement images in the Detection of Myocardial Fibrosis in Hypertrophic Cardiomyopathy Dissertação orientada por. ISMRM Iber Chapter Annu Meet. 2021;

23. Messroghli DR, Radjenovic A, Kozerke S, Higgins DM, Sivananthan MU, Ridgway JP. Modified Look-Locker inversion recovery (MOLLI) for high-resolution T1 mapping of the heart. Magn Reson Med [Internet]. 2004 [cited 2024 Sep 8];52(1):141–6. Available from: https://pubmed.ncbi.nlm.nih.gov/15236377/

24. Tseng WYI, Su MYM, Tseng YHE. Introduction to Cardiovascular Magnetic Resonance: Technical Principles and Clinical Applications. Acta Cardiol Sin [Internet]. 2016 Mar 1 [cited 2024 Sep 8];32(2):129. Available from: /pmc/articles/PMC4816912/

25. Richardson P, McKenna RW, Bristow M, Maisch B, Mautner B, O'Connell J, et al. Report of the 1995 World Health Organization/International Society and Federation of Cardiology Task Force on the Definition and Classification of

Cardiomyopathies. Circulation [Internet]. 1996 Mar 1 [cited 2023 Jul 4];93(5):841–2. Available from: https://www.ahajournals.org/doi/abs/10.1161/01.CIR.93.5.841

26. Ferreira VM, Schulz-Menger J, Holmvang G, Kramer CM, Carbone I, Sechtem U, et al. Cardiovascular Magnetic Resonance in Nonischemic Myocardial Inflammation: Expert Recommendations. J Am Coll Cardiol [Internet]. 2018 Dec 18 [cited 2024 Sep 3];72(24):3158–76. Available from: https://pubmed.ncbi.nlm.nih.gov/30545455/

27. Von Knobelsdorff-Brenkenhoff F, Prothmann M, Dieringer MA, Wassmuth R, Greiser A, Schwenke C, et al. Myocardial T1 and T2 mapping at 3 T: reference values, influencing factors and implications. J Cardiovasc Magn Reson [Internet]. 2013 [cited 2024 Sep 3];15(1):53. Available from: /pmc/articles/PMC3702448/

28. Wassmuth R, Prothmann M, Utz W, Dieringer M, Von Knobelsdorff-Brenkenhoff F, Greiser A, et al. Variability and homogeneity of cardiovascular magnetic resonance myocardial T2-mapping in volunteers compared to patients with edema. J Cardiovasc Magn Reson [Internet]. 2013 [cited 2024 Sep 3];15(1):27. Available from: /pmc/articles/PMC3627620/

29. Baeßler B, Schaarschmidt F, Stehning C, Schnackenburg B, Maintz D, Bunck AC. A systematic evaluation of three different cardiac T2-mapping sequences at 1.5 and 3T in healthy volunteers. Eur J Radiol [Internet]. 2015 Nov 1 [cited 2024 Sep 3];84(11):2161–70. Available from: https://pubmed.ncbi.nlm.nih.gov/26276731/

30. Baeßler B, Schaarschmidt F, Dick A, Stehning C, Schnackenburg B, Michels G, et al. Mapping tissue inhomogeneity in acute myocarditis: a novel analytical approach to quantitative myocardial edema imaging by T2-mapping. J Cardiovasc Magn Reson [Internet]. 2015 Dec 23 [cited 2024 Sep 3];17(1). Available from: /pmc/articles/PMC4690253/

31. Hypertrophic Cardiomyopathy (HCM) | American Heart Association [Internet]. [cited 2024 Aug 12]. Available from: https://www.heart.org/en/health-topics/cardiomyopathy/what-is-cardiomyopathy-in-adults/hypertrophic-cardiomyopathy

32. Freitas P, Ferreira AM, Arteaga-Fernández E, De Oliveira Antunes M, Mesquita J, Abecasis J, et al. The amount of late gadolinium enhancement outperforms current guideline-recommended criteria in the identification of patients with

hypertrophic cardiomyopathy at risk of sudden cardiac death. J Cardiovasc Magn Reson [Internet]. 2019 Aug 15 [cited 2024 Sep 13];21(1). Available from: https://pubmed.ncbi.nlm.nih.gov/31412875/

33. Cardiac MR | Circle Cardiovascular Imaging [Internet]. [cited 2024 Sep 2]. Available from: https://www.circlecvi.com/cardiac-mr

34. Harrigan CJ, Peters DC, Gibson CM, Maron BJ, Manning WJ, Maron MS, et al. Hypertrophic cardiomyopathy: quantification of late gadolinium enhancement with contrast-enhanced cardiovascular MR imaging. Radiology [Internet]. 2011 Jan [cited 2024 Sep 2];258(1):128–33. Available from: https://pubmed.ncbi.nlm.nih.gov/21045187/

35. Maron MS, Appelbaum E, Harrigan CJ, Buros J, Gibson CM, Hanna C, et al. Clinical profile and significance of delayed enhancement in hypertrophic cardiomyopathy. Circ Heart Fail [Internet]. 2008 [cited 2024 Sep 2];1(3):184–91. Available from: https://pubmed.ncbi.nlm.nih.gov/19808288/

36. Małek ŁA, Werys K, Kłopotowski M, Śpiewak M, Miłosz-Wieczorek B, Mazurkiewicz Ł, et al. Native T1-mapping for non-contrast assessment of myocardial fibrosis in patients with hypertrophic cardiomyopathy--comparison with late enhancement quantification. Magn Reson Imaging [Internet]. 2015 Jul 1 [cited 2024 Sep 2];33(6):718–24. Available from: https://pubmed.ncbi.nlm.nih.gov/25863138/

37. Zou KH, O'Malley AJ, Mauri L. Receiver-operating characteristic analysis for evaluating diagnostic tests and predictive models. Circulation [Internet]. 2007 Feb [cited 2024 Sep 13];115(5):654–7. Available from: https://pubmed.ncbi.nlm.nih.gov/17283280/

38. Avard E, Shiri I, Hajianfar G, Abdollahi H, Kalantari KR, Houshmand G, et al. Non-contrast Cine Cardiac Magnetic Resonance image radiomics features and machine learning algorithms for myocardial infarction detection. Comput Biol Med. 2022 Feb 1;141:105145.

39. Wang H, Chen Y, Ma C, Avery J, Hull L, Carneiro G. Multi-modal Learning with Missing Modality via Shared-Specific Feature Modelling. 2023 Jul 26 [cited 2024 Sep 14];15878–87. Available from: https://arxiv.org/abs/2307.14126v2

APPENDICES

Appendix 1 - Results of Initial visual test. D - Detected and ND – Non-detected.

REAL DIAGNOSIS	T1	CINE	LGE
LGE+	D	D	D
LGE+	ND	D	D
LGE+	ND	D	D
LGE+	ND	D	D
LGE+	ND	ND	D
LGE+	D	D	D
LGE+	D	D	D
LGE+	D	D	D
LGE+	ND	ND	D
LGE+	ND	D	D
LGE+	-	ND	D
LGE+	D	ND	D
LGE+	D	D	D
LGE+	D	D	D
LGE+	ND	ND	D
LGE+	D	D	D
LGE+	D	D	D
LGE+	D	ND	ND
LGE-	ND	ND	ND
LGE-	D	ND	ND
LGE-	ND	ND	ND
LGE-	ND	ND	ND
LGE-	ND	ND	ND
LGE-	ND	ND	ND
LGE-	ND	ND	ND
LGE-	D	ND	ND
LGE-	ND	ND	ND
LGE-	ND	ND	ND
LGE-	D	ND	ND
LGE-	ND	ND	ND
LGE-	ND	ND	ND
LGE-	ND	ND	ND
LGE-	ND	ND	ND
LGE-	ND	ND	ND

LGE-	ND	ND	ND
LGE-	ND	ND	ND

Appendix 2 - T1 MAPPING mean values for 17 LGE+ patients, by segment and ROI.

T1 MAPPING VALUES (ms)				
ROI	**SEGMENT1**	**SEGMENT2**	**SEGMENT3**	**SEGMENT4**
1133.46	1114.55	1037.15	1063.41	1113.03
1037.20	1031.86	1016.28	1015.47	1032.07
1048.20; 1116.50	1103.00	1025.02	1041.33	1041.54
1070.82; 1068.26; 1114.05; 1090.24	1050.17	1028.46	1038.97	1035.54
1050.15; 1039.10	1039.38	1030.56	1023.04	1049.47
1107.08	1073.23	1063.49	1037.74	1057.27
1151.66	1128.64	1029.60	1023.31	1118.82
1157.59	1075.13	1081.56	1117.74	1066.22
1088.10	1048.37	1044.29	1046.62	1065.00
1081.32	1070.02	1047.30	1091.80	1058.39
1178.36	1024.17	1008.10	992.307	1046.67
1076.59	1062.09	1030.03	994.713	1005.54
1152.30	1046.71	1145.96	1035.05	1082.01
1179.47; 1258.65	1126.72	115.06	1249.41	1171.16
1003.93	1064.97	1018.24	1024.77	1046.57
1087.20	1084.16	1077.13	1025.48	1040.20
1171.00	1113.23	1058.50	1037.50	1106.18

Appendix 3 - Representation of the positive segments and number of ROIs in LGE+ patients, in LGE images. Positive segments (LGE+) were placed in bold for better visualization.

ROIs	**SEGMENT 1**	**SEGMENT 2**	**SEGMENT 3**	**SEGMENT 4**
1	**LGE+**	LGE-	LGE-	LGE-
1	**LGE+**	**LGE+**	LGE-	LGE-
2	**LGE+**	LGE-	LGE-	LGE-
4	**LGE+**	**LGE+**	**LGE+**	**LGE+**

1	LGE-	LGE-	LGE-	**LGE+**
1	**LGE+**	**LGE+**	LGE-	LGE-
1	**LGE+**	LGE-	LGE-	**LGE+**
1	LGE-	LGE-	**LGE+**	LGE-
1	LGE-	LGE-	LGE-	**LGE+**
1	**LGE+**	LGE-	LGE-	LGE-
1	**LGE+**	LGE-	LGE-	LGE-
1	**LGE+**	**LGE+**	LGE-	LGE-
1	LGE-	LGE-	LGE-	**LGE+**
2	**LGE+**	LGE-	**LGE+**	**LGE+**
1	LGE-	**LGE+**	**LGE+**	LGE-
1	**LGE+**	**LGE+**	LGE-	LGE-
1	**LGE+**	LGE-	LGE-	LGE-
1	LGE-	LGE-	LGE-	**LGE+**

Appendix 4 - CINE mean and area values for 18 LGE+ patients, by segment and ROI. The weighted mean values were calculated with these values.

CINE IMAGING VALUES					
ROI	**AREA (CM2)**	**SEGMENT1**	**SEGMENT2**	**SEGMENT3**	**SEGMENT4**
149.420	13.060/6.523/5.640/10.641	142.068	141.811	158.701	149.539
163.894	6.234/4.988/4.274/4.961	151.950	137.060	131.177	141.032
145.509 148.206	6.329/5.632/4.217/4.999	139.580	134.512	156.294	151.599
149.073 156.148 148.644 147.598	6.004/5.284/3.636/4.570	141.887	136.176	152.827	154.914
130.134 85.155	7.121/6.281/5.687/6.988	88.690	94.241	117.758	113.377

99.800	10.468/9.660/8.427/5.887	102.321	103.910	101.245	108.577
169.090	7.578/4.743/6.061/11.743	153.269	141.762	147.537	155.153
70.640	5.560/6.200/5.745/5.300	49.776	46.475	59.680	54.212
99.772	3.976/3.002/2.765/3.754	91.967	90.314	103.924	97.981
77.814	7.008/4.743/4.267/5.117	67.380	48.908	71.374	44.808
110.602	5.903/4.015/2.864/3.636	107.313	101.519	121.521	113.315
102.946	6.664/4.117/5.028/5.083	103.445	109.217	108.603	118.852
66.851	6.917/6.747/3.277/3.744	71.447	72.518	79.889	82.152
142.040	3.827/3.608/3.357/3.585	98.241	119.081	108.120	115.645
181.291	5.106/2.955/4.507/4.018	129.764	137.976	174.287	151.201
137.903					
144.975	5.432/6.322/6.528/5.773	117.120	131.189	139.027	126.980
105.184	15.340/9.315/11.633/12.212	101.062	102.493	101.035	93.993
142.068	5.861/5.207/2.792/3.310	129.351	117.722	119.507	129.809

Appendix 5 - Weighted Mean values calculated, used as reference.

ROI	Weighted Mean Values	SEG+
149.415	149.594	142.068
163.894	136.471	151.955/137.06
145.509	146.451	139.583
148.206		
149.073	126.540	141.887/136.176/152.827/154.914
156.148		
148.644		
147.598		
130.134	101.597	94.241/113.377
85.155		
99.800	104.260	102.321/103.910
169.090	145.002	153.269/155.153
70.640	49.954	59.680
99.772	94.852	97.981
77.814	54.208	67.380
110.602	111.046	107.313
102.946	106.589	118.852
66.851	81.096	71.447/72.518
142.040	108.281	115.645

181.291 137.903	137.976	129.764/174.287
144.975	122.200	131.189/139.027
105.184	97.428	101.062/102.493
142.068	121.700	129.351

Appendix 6 - Results of Blind test with segment identified. D - Detected and ND – Non-detected.

REAL DIAGNOSIS	T1	CINE
LGE+ (SEG1)	D (SEG1)	D (SEG1)
LGE+ (SEG1/2)	D (SEG1/2)	D (SEG1/2)
LGE-	ND	ND
LGE-	D (SEG4)	D (SEG4)
LGE+ (SEG1)	ND	D (SEG2/3)
LGE-	ND	ND
LGE+ (ALL SEG)	ND	ND
LGE+ (SEG4)	ND	D (SEG3/4)
LGE-	ND	ND
LGE-	ND	ND
LGE+ (SEG1/2)	ND	ND
LGE+ (SEG1/4)	D (SEG4)	D (SEG4)
LGE+ (SEG3)	D (SEG3)	D (SEG3)
LGE-	ND	ND
LGE+ (SEG4)	D (SEG4)	D (SEG4)
LGE-	ND	ND
LGE+ (SEG1)	ND	D (SEG1)
LGE+ (SEG4)	D (SEG4)	ND
LGE+ (SEG1/2)	D (SEG1/2)	ND
LGE-	D (SEG1/2)	ND
LGE-	ND	ND
LGE-	ND	D (SEG3)
LGE-	ND	ND
LGE-	ND	ND
LGE+ (SEG4)	D (SEG2/3)	D - seg2/3
LGE+ (SEG1/3/4)	D (ALL SEG)	D (ALL SEG)
LGE+ (SEG2/3)	D (SEG2/3)	D (SEG2/3)
LGE-	D (SEG1)	ND

LGE+ (SEG1/2)	D (SEG1)	D (SEG1/3/4)
LGE-	ND	ND